

## TRIGGERING THE MAGNETOPAUSE RECONNECTION BY SOLAR WIND DISCONTINUITIES

ALEXANDER LUKIN,<sup>1,2</sup> ZHIFANG GUO,<sup>3,4</sup> YU LIN,<sup>4</sup> EVGENY PANOV,<sup>5</sup> ANTON ARTEMYEV,<sup>6,1</sup>  
XIAOJIA ZHANG,<sup>7,6</sup> AND ANATOLI PETRUKOVICH<sup>1</sup>

<sup>1</sup>*Space Research Institute, RAS, Moscow, Russia*

<sup>2</sup>*Faculty of Physics, National Research University Higher School of Economics, Moscow, Russia*

<sup>3</sup>*School of Geophysics and Information Technology, China University of Geosciences, Beijing, China*

<sup>4</sup>*Physics Department, Auburn University, Auburn, AL, USA*

<sup>5</sup>*Space Research Institute, Austrian Academy of Sciences, Schmiedlstrasse 6, 8042 Graz, Austria*

<sup>6</sup>*Department of Earth, Planetary, and Space Sciences and Institute of Geophysics and Planetary Physics, University of California, Los Angeles, CA, USA*

<sup>7</sup>*Department of Physics, University of Texas at Dallas, Richardson, TX, USA*

(Received December 7, 2023)

Submitted to ApJ

### ABSTRACT

Magnetic reconnection is one of the most universal processes in space plasma that is responsible for charged particle acceleration, mixing and heating of plasma populations. In this paper we consider a triggering process of reconnection that is driven by interaction of two discontinuities: solar wind rotational discontinuity and tangential discontinuity at the Earth's magnetospheric boundary, magnetopause. Combining the multispacecraft measurements and global hybrid simulations, we show that solar wind discontinuities may drive the magnetopause reconnection and cause the mixing of the solar wind and magnetosphere plasmas around the magnetopause, well downstream of the solar wind flow. Since large-amplitude discontinuities are frequently observed in the solar wind and predicted for various stellar winds, our results of reconnection driven by the discontinuity-discontinuity interaction may have a broad application beyond the magnetosphere.

*Keywords:* solar wind – turbulence, magnetopause, reconnection, hybrid simulation

## 1. INTRODUCTION

Magnetohydrodynamic (MHD) discontinuities are basic solutions for boundaries of plasmas with different properties (Landau & Lifshitz 1960; Hudson 1970), and are fundamental element of space plasma flows, e.g., solar wind (Tsurutani & Ho 1999) and stellar winds (Arons 2012; Sironi & Spitkovsky 2011). Such discontinuities are considered as elementary blocks of MHD turbulence (Servidio et al. 2011b; Matthaeus et al. 2015; Loureiro & Boldyrev 2017) and serve as a primary framework for magnetic field line reconnection, a major process responsible for the transfer of magnetic field energy to plasma heating and charged particle acceleration (Birn & Priest 2007; Gonzalez & Parker 2016; Pontin & Priest 2022). Besides the spontaneous magnetic reconnection due to discontinuity instability (Syrovatskii 1981; Loureiro et al. 2007; Pucci & Velli 2014), magnetic reconnection can be driven by an interaction of two discontinuities. The most investigated type of such driven reconnections is that due to interaction of a tangential discontinuity and a shock wave (see examples of simulations for astrophysical and solar plasma systems in, e.g., Phan et al. 2007; Sironi & Spitkovsky 2012; Matsumoto et al. 2015; Omidi et al. 2009; Guo et al. 2018, 2021a,b). Numerical simulations and theoretical models of discontinuity interactions associated with magnetic reconnection are largely motivated by multiple spacecraft observations in the near-Earth space environment and in the solar wind, the natural laboratory of plasma dynamics.

Earth's bow shock and magnetopause are formed by solar wind interaction with the Earth's dipole field and are separated by the magnetosheath, the region filled by subsonic (shocked) plasma flow. The magnetosheath-magnetosphere boundary, magnetopause, can be described as a tangential discontinuity (De Keyser et al. 2005), an equilibrium current sheet where the geomagnetic field lines are 'closed'. Solar wind flow transport kinetic-scale discontinuities (see statistical properties of such discontinuities in Söding et al. 2001; Vasquez et al. 2007; Artemyev et al. 2018; Vasko et al. 2021) sharing properties of both rotational and tangential discontinuities (Neugebauer 2006; Artemyev et al. 2019) and carrying strong current density (Podesta 2017; Greco et al. 2016; Newman et al. 2020). Interaction of solar wind discontinuities with the bow shock significantly modifies the discontinuity structure (Yan & Lee 1996; Lin et al. 1996a; Cable & Lin 1998) and can also produce various types of magnetosheath perturbations: plasma bubbles (Liu et al. 2015; An et al. 2020; Vu et al. 2022), density cavities (Lin 2003; Lin & Wang 2005; Sibeck et al. 2002, 2021; Omidi et al. 2013), hot flow anomalies (Lin 1997, 2002; Omidi & Sibeck 2007; Omidi et al. 2016), and plasma pressure pulses (Hubert & Harvey 2000; Farrugia et al. 2018). Both modification of the initial discontinuity configuration and generation of magnetosheath perturbations involve ion kinetic processes, and thus are well reproduced by hybrid simulations treating ions as particles and electrons as a fluid (e.g., Lin et al. 1996a,b; Lin & Wang 2005; Omidi et al. 2016, 2020; Ng et al. 2021; Chen et al. 2021).

Schematic 1 shows main types of magnetic reconnections observed within the day-side Earth's magnetosphere environment: reconnection at solar wind discontinuities (Farrugia et al. 2001; Gosling 2012; Phan et al. 2006), reconnection due to the discontinuity interaction with the bow shock (Pang et al. 2010; Vörös et al. 2017; Wang et al. 2019; Gingell et al. 2019, 2020; Guo et al. 2021b), and reconnection on the magnetopause (Paschmann et al. 1979, 2013; Phan et al. 2014; Burch et al. 2016). The latter one is generally driven by a change of the interplanetary magnetic field direction, i.e. by solar wind discontinuity arriving to the magnetopause. In this study we focus on this last type of reconnection associated with magnetopause interaction with magnetosheath perturbations, in which the sheath perturbations are generated by the solar wind discontinuity interaction with

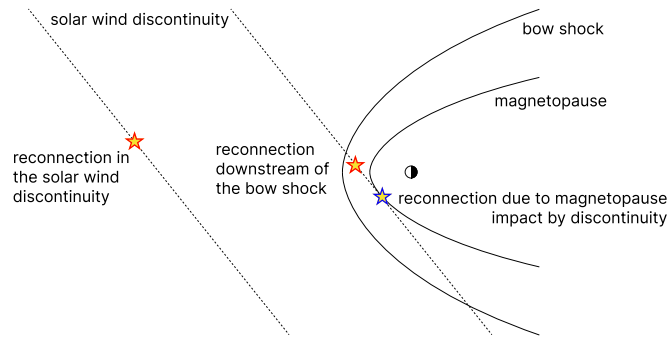


**Figure 1.** Schematic view of main types of magnetic reconnection associated with the solar wind discontinuities.

the bow shock. We consider very coherent perturbations, and study the magnetopause (that is tangential discontinuity, see Roth et al. (1996); De Keyser et al. (2005)) interaction with the solar wind rotational discontinuity modified by the passage through the bow shock (that is the shock-type discontinuity).

One of the important consequences of discontinuity interaction with the bow shock is its compression with the significant increase of the current density (Phan et al. 2007; Webster et al. 2021; Kropotina et al. 2021). Therefore, such amplified discontinuities should be more unstable to magnetic reconnection in the magnetosheath. Indeed, recent observations (Vörös et al. 2017; Wang et al. 2019; Gingell et al. 2019, 2020) and kinetic simulations (Guo et al. 2018) show reconnection signatures downstream of the Earth’s bow shock, and such reconnection is associated with the tangential discontinuity interaction with the bow shock. However, reconnection does not necessary destroy the current layer, which can reach the magnetopause. Rotational discontinuities are especially stable to magnetic reconnection (see Discussion for more details). Interaction between the modified rotational discontinuity and the magnetopause, that is a tangential discontinuity, may also drive the magnetic field line reconnection and magnetosheath-magnetosphere plasma exchange. This type of reconnection is in focus of our study.

Roles of various magnetosheath perturbations in the magnetopause dynamics is well documented by in-situ spacecraft measurements (e.g., Sibeck et al. 2000; Jacobsen et al. 2009; Archer et al. 2014; Hietala et al. 2018) and ground-based magnetometers (e.g., Archer et al. 2015). Moreover, such dynamics results in the generation of a broad range of ultra-low-frequency (MHD) waves within the Earth’s magnetosphere, and these waves are usually detected by the ground-based and spacecraft magnetic field and plasma measurements (e.g., Wang et al. 2018a, 2020a; Shi et al. 2021). Such magnetosheath perturbations may propagate from the day-side to midtail magnetosheath (Wang et al. 2018b) and drive the flank magnetopause dynamics (Wang et al. 2020b). Therefore, we shall consider possibility of both day-side and night-side (flank) magnetopause reconnection driven by the solar wind discontinuity crossing the bow shock.

In this study we combine the 3D global hybrid simulation (see model description in Lin & Wang 2005) of the interaction between the magnetopause and the solar wind discontinuities with THEMIS (Angelopoulos 2008), MMS (Burch et al. 2016), and ARTEMIS (Angelopoulos 2011) observations to investigate the subsequent discontinuity interaction with the magnetopause and driven magnetopause reconnection. Our main event describes the day-side reconnection, and for this event we use the simulation results to confirm our interpretation of ARTEMIS and THEMIS measurements. The second

event describes ARTEMIS and MMS observations of night-side magnetopause reconnection driven by a solar wind discontinuity. We use this event to demonstrate that discontinuity-magnetopause interaction may drive magnetic reconnection in different plasma flow configurations. We also analyze three supplementary events with magnetopause crossings before and after the solar wind discontinuity impact, which confirm that the solar wind discontinuity impact may trigger magnetic reconnection at the initially non-reconnected magnetopause.

## 2. SPACECRAFT OBSERVATIONS

### 2.1. Data and methods

Below we show two events of interaction between solar wind rotational discontinuities and the Earth's magnetopause. We use the data obtained onboard THEMIS/ARTEMIS (Angelopoulos 2008, 2011) and MMS (Burch et al. 2016) missions. THEMIS/ARTEMIS fluxgate magnetometers (Auster et al. 2008) and electrostatic analyzers (ESA; McFadden et al. (2008)) provide us with the magnetic field vector, moments of ion and electron distribution functions (number density, temperatures and bulk velocities) and phase space density measurements with a spin time resolution (3 and 4 second for THEMIS and ARTEMIS respectively). MMS fluxgate magnetometer (Russell et al. 2016) measurements are available with 1/16s resolution, while the plasma moments measured by Fast Plasma Investigation (FPI) instrument (Pollock et al. 2016) are provided with 4.5 seconds resolution.

To restore the local (lmn) coordinate system of the discontinuity we use the minimum variance analysis (MVA; Sonnerup & Scheible (2000)). To estimate the spatial scale of the discontinuity we use almost the same single-spacecraft technique as proposed by Haaland & Gjerloev (2013), but since the MVA often does not distinguish between the intermediate and normal directions we use the velocity component perpendicular to the main magnetic field ( $l$ ) component,  $\mathbf{v}_{mn} = \mathbf{v} - (\mathbf{v} \cdot \mathbf{e}_l)\mathbf{e}_l$  in our analysis, i.e. we may overestimate the discontinuity thickness  $L = \Delta t|\mathbf{v}_{mn}|$  ( $\Delta t$  is the time interval of discontinuity crossing by spacecraft).

For steady reconnection process under symmetrical boundary conditions and a finite guide field, there exist two symmetrical rotational discontinuities bounding the outflow region, and thus we expect that the variation of the plasma flow velocity across the outflow region discontinuities should satisfy the Walen relation  $\Delta\mathbf{v} = \pm\Delta\mathbf{B}/(4\pi\rho)$  (Parker 1957; Petschek 1964; Lin & Lee 1993). The magnetopause reconnection however, are usually characterized by asymmetrical boundary conditions (Phan et al. 2007, 2014) so the jump of plasma flow speed should be comparable to the asymmetric Alfvén speed  $v_{Al,asym}$  (Cassak & Shay 2007; Swisdak & Drake 2007):

$$v_{Al,asym}^2 = \frac{B_{l1}B_{l2}(B_{l1} + B_{l2})}{4\pi(\rho_1B_{l2} + \rho_2B_{l1})}, \quad (1)$$

where  $B_{l1,2}$ ,  $\rho_{1,2}$  are the values of anti-parallel reconnecting magnetic field component and plasma density on both sides of the outflow region boundaries. In our selected events, spacecraft do not cross the reconnecting magnetopause, but observe the discontinuities likely connecting to the magnetopause reconnection side. Therefore, we may not estimate the magnetic field configuration of the reconnecting magnetopause, and we use component-wise estimates of the asymmetrical Alfvén speed  $v_{Aj,asym}^2 = (B_{j1}B_{j2}(B_{j1} + B_{j2}))/4\pi(\rho_1B_{j2} + \rho_2B_{j1})$ , where  $j = x, y, z$  (we use GSM coordinate system through the paper), and  $B_{j1}$ ,  $\rho_1$  and  $B_{j2}$ ,  $\rho_2$  are measured in the magnetosheath near the discontinuity and in the magnetosphere.

## 2.2. Day-side event

Figure 2 shows an overview of the event with the day-side magnetopause reconnection driven by the solar wind discontinuity. THEMIS C (ARTEMIS P2) is in the solar wind, upstream of the bow shock (see panels (l), (m)), and observes a series of the solar wind discontinuities (shaded in red in Fig. 2(a),(b)) at  $\sim 12:41$ ,  $\sim 12:44$ ,  $\sim 12:55$  and  $\sim 13:10$  with the magnetic field rotation mostly seen in GSM  $B_x$ ,  $B_z$  for the first and second events, and in GSM  $B_y$ ,  $B_z$  for in the third and fourth events. The magnetic field rotation is accompanied by jumps of solar wind flow  $\Delta v_{x,y,z} \approx B_{x,y,z}/\sqrt{4\pi\rho}$  (not shown) with the almost constant field magnitude  $|B|$ . These are typical properties of rotational discontinuity (Tsurutani & Ho 1999; Neugebauer 2006). Although single spacecraft measurements do not allow to check the normal magnetic field component with necessary accuracy (see Knetter et al. 2004), we use the time delay of discontinuity measurements by two ARTEMIS spacecraft to improve accuracy of MVA (see details of this method in Artemyev et al. 2019) and estimate a normal magnetic field component:  $B_n/\Delta B_l \approx (0.2, 0.1, 0.1, 0.05)$  for four discontinuities shown in Fig. 2. For three first discontinuities  $B_n$  is quite comparable to the  $B_l$  change across the discontinuity (the discontinuity amplitude), and thus we can confirm that these are rotational discontinuities. Their spatial scales (thicknesses) in the solar wind, based on THEMIS C observations, are  $L_1 \sim 7500\text{km}$ ,  $L_2 \sim 6200\text{km}$ ,  $L_3 \sim 3050\text{km}$  and  $L_4 \sim 2200\text{km}$ .

These rotational discontinuities cross the bow shock and are observed downstream (in the magnetosheath) by THEMIS D and E. The interaction with the bow shock compresses the discontinuity and increases the magnetic field amplitude from  $\sim 5\text{nT}$  in the solar wind to  $\sim 20 - 30\text{nT}$  in the magnetosheath. The spatial scales of these discontinuities in the magnetosheath, based on THEMIS D and E observations, are  $L_{1d} \sim 2000\text{km}$ ,  $L_{2d} \sim 5300\text{km}$ ,  $L_{3d} \sim 1500\text{km}$ ,  $L_{4d} \sim 550\text{km}$  and  $L_{1e} \sim 2500\text{km}$ ,  $L_{2e} \sim 7600\text{km}$ ,  $L_{3e} \sim 2000\text{km}$ ,  $L_{4e} \sim 800\text{km}$ . Such intensification of discontinuities downstream of the bow shock has been reproduced in simulations (e.g., Yan & Lee 1996; Lin et al. 1996a; Guo et al. 2018, 2021b,a; Kropotina et al. 2021) and reported in spacecraft observations (e.g., Webster et al. 2021; Kropotina et al. 2021). The interesting aspect of the discontinuity observation in the magnetosheath is the population of energetic ions (mostly seen around the last discontinuity). Energy spectrum clearly shows this population at  $> 5\text{keV}$  range, significantly higher than the shocked solar wind energies. The pitch-angle distribution of this population indicates that energetic ions are moving along magnetic field lines (not shown), i.e. along  $-y$  direction from the magnetopause. Therefore, this may be a leakage of the magnetospheric population (for which  $5 - 15\text{keV}$  energy range is expected). Such observations in the magnetosheath suggest that discontinuity are connected to the magnetopause reconnection region. The scenario for such observations includes the discontinuity impact on the magnetopause, local reconnection between the magnetosheath and magnetospheric field lines, and ion leakage along the reconnected magnetic field lines (along the discontinuity surface) to the magnetosheath, where this magnetospheric ion population is observed in association with the discontinuities. An alternative, or rather supplementary mechanism can be the magnetospheric plasma leakage into the magnetosheath due to magnetosphere compression by the pressure pulse formed by the discontinuity interaction with the bow shock (see Lin et al. 1996b; Archer et al. 2012). Such a compression may release magnetospheric plasma into magnetosheath and may drive the magnetopause reconnection (e.g., Hietala et al. 2018).

Before the discontinuity arrives to the magnetopause, THEMIS A was inside the magnetosphere (the magnetopause crossing from the magnetosheath to the magnetosphere occurs at  $\sim 12:05$ ) and

observed almost stationary magnetic field, stagnant plasma, low plasma density, and hot ions (before 13:17). Then THEMIS A detected several injections of the cold dense magnetosheath plasma into the magnetosphere: increase of density, low-energy population in ion and electron spectra, magnetic field perturbations. These injections of cold plasma are accompanied by observations of plasma jets seen as bipolar flows around  $\sim 12:57$ ,  $\sim 13:18$  and  $\sim 13:22$ . The component-wise estimates of asymmetric Alfvén speed calculated for all marked discontinuities are  $v_{Ax,asym} \sim 50 - 70 \text{ km/s}$ ,  $v_{Ay,asym} \sim 20 - 30 \text{ km/s}$ ,  $v_{Az,asym} \sim 90 - 120 \text{ km/s}$  and comparable to the observed jet speeds. Therefore, we may suggest that discontinuity’s impact on the magnetopause triggers magnetic reconnection that is responsible for the magnetosheath plasma penetration into the magnetosphere and the magnetospheric plasma penetration into the magnetosheath. This impact (and magnetic reconnection) also drives MHD waves propagating away from the magnetopause and observed by THEMIS A as quasi-periodic  $v_x$  variations modulating the cold ion and electron populations after 13:22:00 (see discussion of such waves in Hartinger et al. 2013; Zhang et al. 2020; Wright & Elsden 2020).

To investigate details of the discontinuity interaction with the magnetopause, we zoom in THEMIS A observations and add information about ion kinetics in Fig. 3. Pitch-angle distributions of thermal ( $< 2 \text{ keV}$ ) and hot ( $\in [4, 20] \text{ keV}$ ) ions show that the bipolar  $v_z$  signature around 13:17-13:19 consists of cold (magnetosheath) ions flowing parallel and hot (magnetospheric) ions flowing anti-parallel to the background magnetic field. This result resembles well the bipolar (reversal) plasma flows from the asymmetric magnetopause reconnection (see review by Paschmann et al. 2013, and references therein), i.e. THEMIS A may have crossed the outflow region of reconnection. Comparison of velocity distributions collected before 12:55 (subinterval #1), during observations of  $v_z > 0$  (subintervals #2 and #3), and well after the bipolar  $v_z$  (subinterval #6) shows that magnetospheric plasma (subinterval #1,6) are predominantly field-aligned anisotropic, whereas injected magnetosheath plasma (subintervals #2, #3 and #5) is transversely anisotropic (both these types of anisotropy are quite typical for the magnetosphere and magnetosheath, see Gary et al. (1995); Samsonov et al. (2007) showing that magnetosheath plasma generally has  $T_{\perp}/T_{\parallel} > 1$ , and Wang et al. (2013) showing the magnetospheric thermal plasma often has  $T_{\parallel} > T_{\perp}$ ). Therefore, Fig. 3 further confirms that THEMIS A observed signatures of magnetic reconnection at the magnetopause: bipolar  $v_z$  pulses and injection of cold magnetosheath plasma into the magnetosphere. This reconnection triggers the MHD (ultra-low-frequency) waves that quasi-periodically brings the magnetosheath population (likely entered into magnetosphere through the reconnected magnetopause) to THEMIS A location via  $\mathbf{E} \times \mathbf{B}$  drift, as shown in the cold transversely anisotropic population in the distribution functions measured during subinterval #2-5.

### 2.3. Night-side event

To investigate a possibility for a solar wind discontinuity to trigger the night-side (flank) magnetopause reconnection, we consider MMS and THEMIS observations during 2021-03-01 event shown in Fig. 4. MMS upstream of the bow shock observes several solar wind discontinuities: large scale magnetic field rotation between 04:35 and 04:50 (marked as 1 in panel (a) of Fig. 4), smaller scale rotation between 04:52 and 04:56 (marked as 2) and a series of  $B_z$  reversals between 06:00 and 06:20 (marked as 3). The spatial scale of the first discontinuity estimated from MMS1 data is about  $10^5$  km. In fact this structure consists of several embedded discontinuities with spatial scales of 11700, 23500 and 9800 km. The second discontinuity have a spatial scale of about 7400 km and consists of two adjacent discontinuities with estimated scales of 2000 and 1900 km. The last marked interval

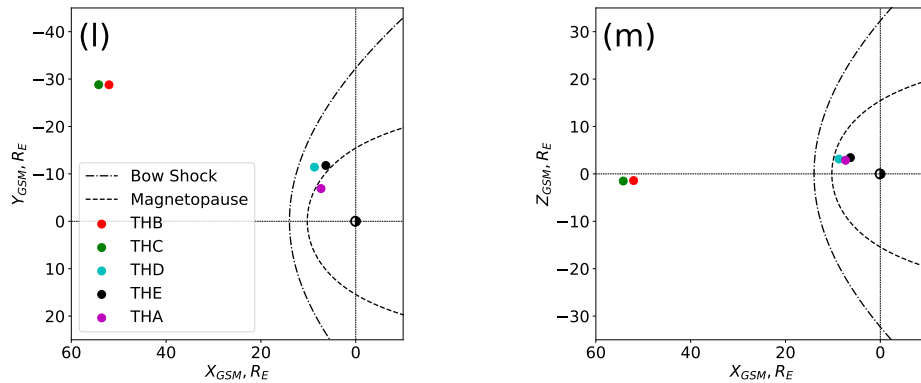
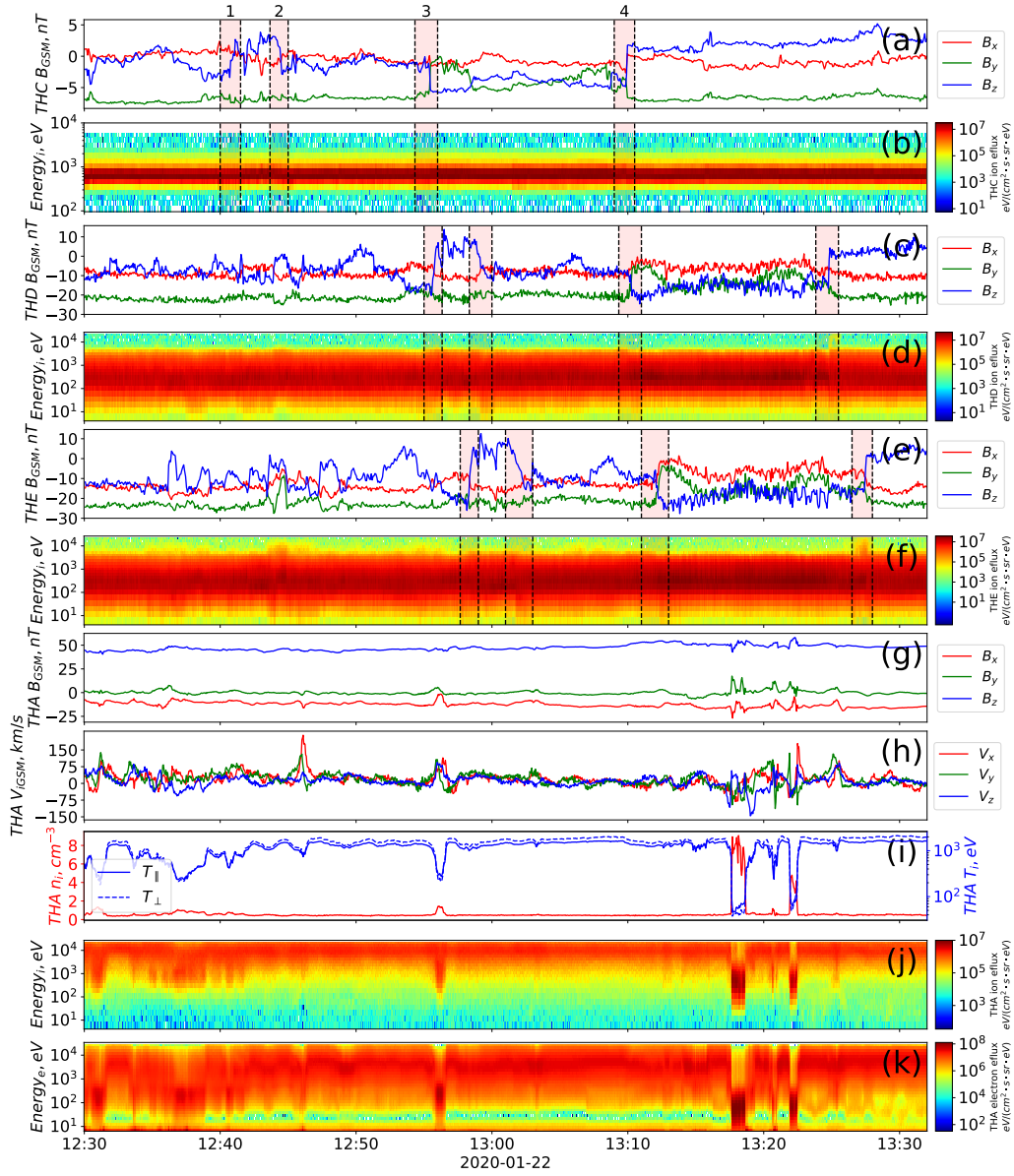


**Figure 2.** The overview of THEMIS observations on 2020-01-22. (a),(b): solar wind discontinuity (magnetic field and ion spectrum on THEMIS C), (c)-(f): the same discontinuity observed downstream of the bow shock (magnetic fields and ion spectra on THEMIS D&E), (g)-(k) magnetospheric observations (magnetic fields, plasma flow velocities, electron density and temperature, ion and electron spectra on THEMIS A). Panels (l) and (m) show spacecraft location in  $XY$  and  $XZ$  GSM planes relative to the model bow shock (Wu et al. 2000) and magnetopause (Shue et al. 1997).

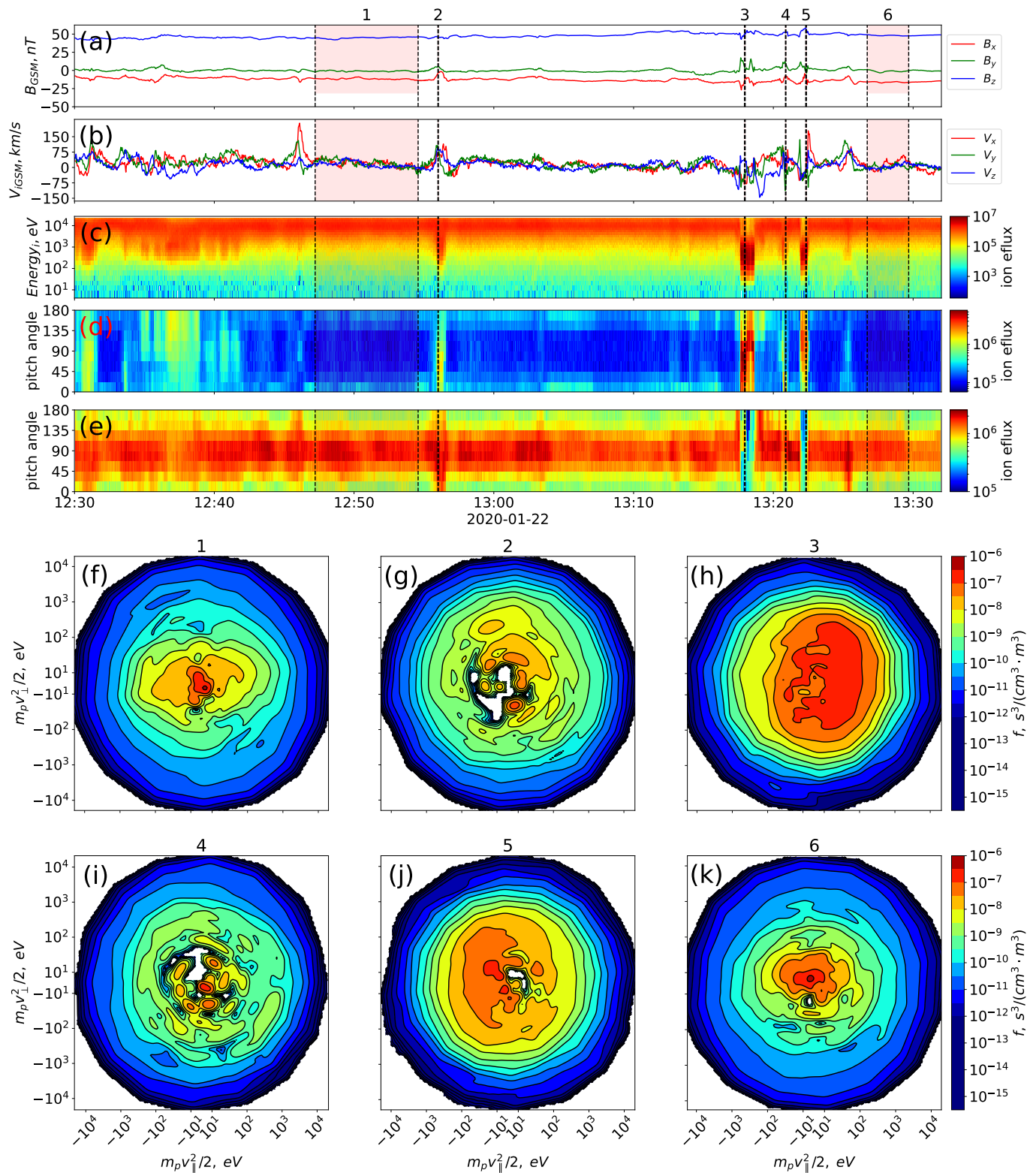


**Figure 3.** The overview of the solar wind discontinuity interaction with the magnetopause observed by THEMIS A: magnetic field components (a), ion flow components (b), ion energy spectrum (c), ion pitch-angle distributions for different energy ranges ([100 – 2000] eV for (d), and [4 – 20] keV for (e)), 2D cuts of ion distributions in  $(m_p v_{\parallel}^2/2, m_p v_{\perp}^2/2)$  plane for several intervals indicated by numbers.



includes several  $B_z$  reversals, the first one, observed at 06:03, have a spatial scale of about 31000 km and consists of two smaller scale discontinuities with scales of 6200 and 1800 km. The one, observed at 06:15, has spatial scale of 5800 km and doesn't appear in the magnetosheath and nigh-side observations.

Each discontinuity is accompanied by solar wind velocity jump (not shown). The same series of discontinuities is observed by THEMIS D downstream of the bow shock in the dayside magnetosheath. Discontinuities are compressed at the bow shock: the magnetic field increases from 10nT in the solar wind to  $\sim 40$ nT in the dayside magnetosheath (THEMIS D). Spatial scale decreases to 35000 km (2500 + 4000 + 6800 km) for the first group of discontinuities, 1200 km for the second discontinuity, and 18000 km (4200+4800 km) for the third group of discontinuities. Note the downstream of the day side bow shock is further compressed by plasma flow breaking at the magnetoapuse, and this results in large discontinuity magnitude increase (see discussion in [Kropotina et al. 2021](#)). Thus, it would be interesting to check the discontinuity effect on the night side magnetosheath (see examples confirming such propagation of solar wind discontinuities to the night-side magnetopause in, e.g., [Wang et al. 2018c, 2020c](#)), where magnetopause surface is almost parallel to the plasma flow [Hasegawa \(2012\)](#); [Lukin et al. \(2019\)](#).

THEMIS B and C (ARTEMIS P1 and P2) show several discontinuities in the night side magnetosheath (downstream from the bow shock,  $\sim 50$  Earth radii away from the day side THEMIS D observations). These discontinuities are only weakly compressed by the bow shock: magnetic field magnitude increases from 10nT to 15nT and discontinuity spatial scales stay almost the same or even increase:  $10^5$  km (11000 + 17000 + 12400 km) for the first group of discontinuities, 9000 km for the second discontinuity, and 64000 km (22000 + 15000 km) for the third group of discontinuities. Note a typical ion thermal gyroradius in the shocked solar wind (in the magnetosheath) is  $\sim 100$ km for cold ions and  $\sim 1000$ km for hot (magnetospheric) ions. Thus small-scale discontinuities are ion kinetic structures for hot ions, but is quite thick for cold magnetosheath ions.

THEMIS C and B cross the magnetopause at 03:50 and 04:05 (a clear change in ion spectra is seen in Fig. 4(g,j)), and after the magnetopause crossing both THEMIS B and C stably measure magnetosheath plasma. However, there are several bursts of hot magnetospeheric ion population on the magnetosheath side around discontinuities, between 05:12 and 05:20, 06:20 and 07:00. In Fig. 5 we describe details of these hot plasma bursts associated with discontinuities. For reference we use ion velocity distributions measured within the magnetosphere (interval #1 in Fig. 5(f)) and in the quiet magnetosheath (intervals #2,3,5 in Fig. 5(g,h,j)): the magnetospheric population is characterized by a finite  $\sim 10$  keV fluxes isotropically distributed in ( $\parallel, \perp$ ) energy space, whereas the magnetosheath population is characterized by large amplitude fluxes of field-aligned flow ( $E_{\parallel} \sim 1$ keV). During interval #4 (the first group of discontinuities) ion distribution function shows a combination of magnetosheath (flowing) and magnetospheric (hot isotropic) plasmas. Pitch-angle distributions in Fig. 5(d,e) confirms that discontinuities are associated with appearance of hot isotropic ion population. A similar picture is observed for the third group of discontinuities (interval #6): pitch-angle distributions and velocity distribution show an appearance of a population of hot ( $\sim 10$  keV) isotropic magnetospheric plasma (see Fig. 5(d,e, k)). Observation of magnetospheric plasma far from the magnetopause (deep inside the magnetosheath) in association with discontinuities suggest that THEMIS C&B cross field lines connecting to the reconnected magnetopause, i.e. there is a magnetic reconnection in regions where these discontinuities impact to the magnetopause.

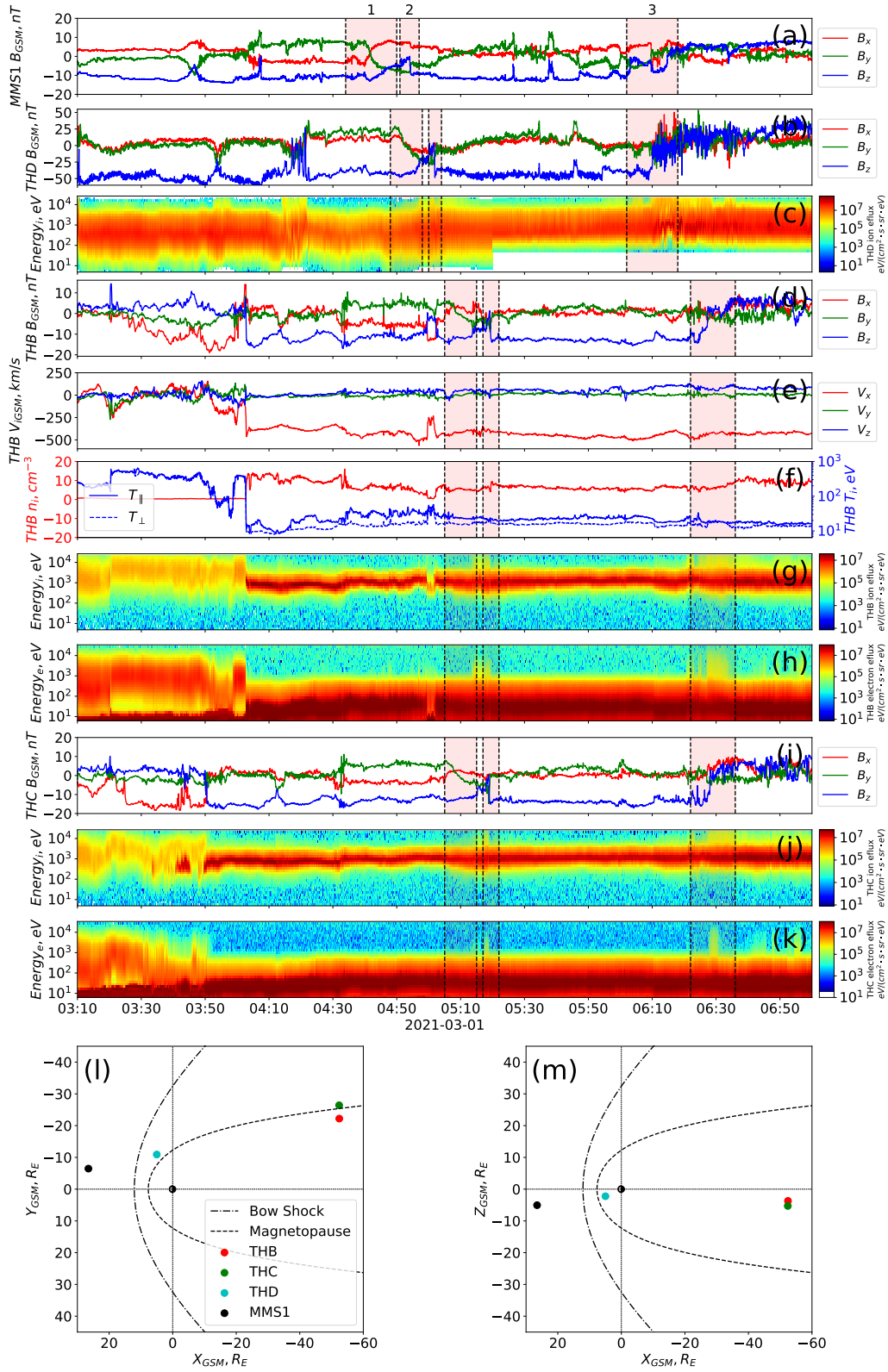


**Figure 4.** The overview of MMS&THEMIS&ARTEMIS observations on 2021-03-01. From top to bottom: (a) solar wind discontinuity (magnetic field on MMS#1), the same discontinuity observed downstream of the bow shock (magnetic fields (b) and ion spectra (c) on THEMIS D), magnetic fields observed downstream of the flank bow shock ((d) for THEMIS B & (i) for THEMIS C), plasma flow velocities on THEMIS B (e), electron density and temperature on THEMIS B (f), ion and electron spectra on ((g, j) for THEMIS B & (h, k) for THEMIS C). Bottom panel shows spacecraft location relative to the model bow shock and magnetopause.

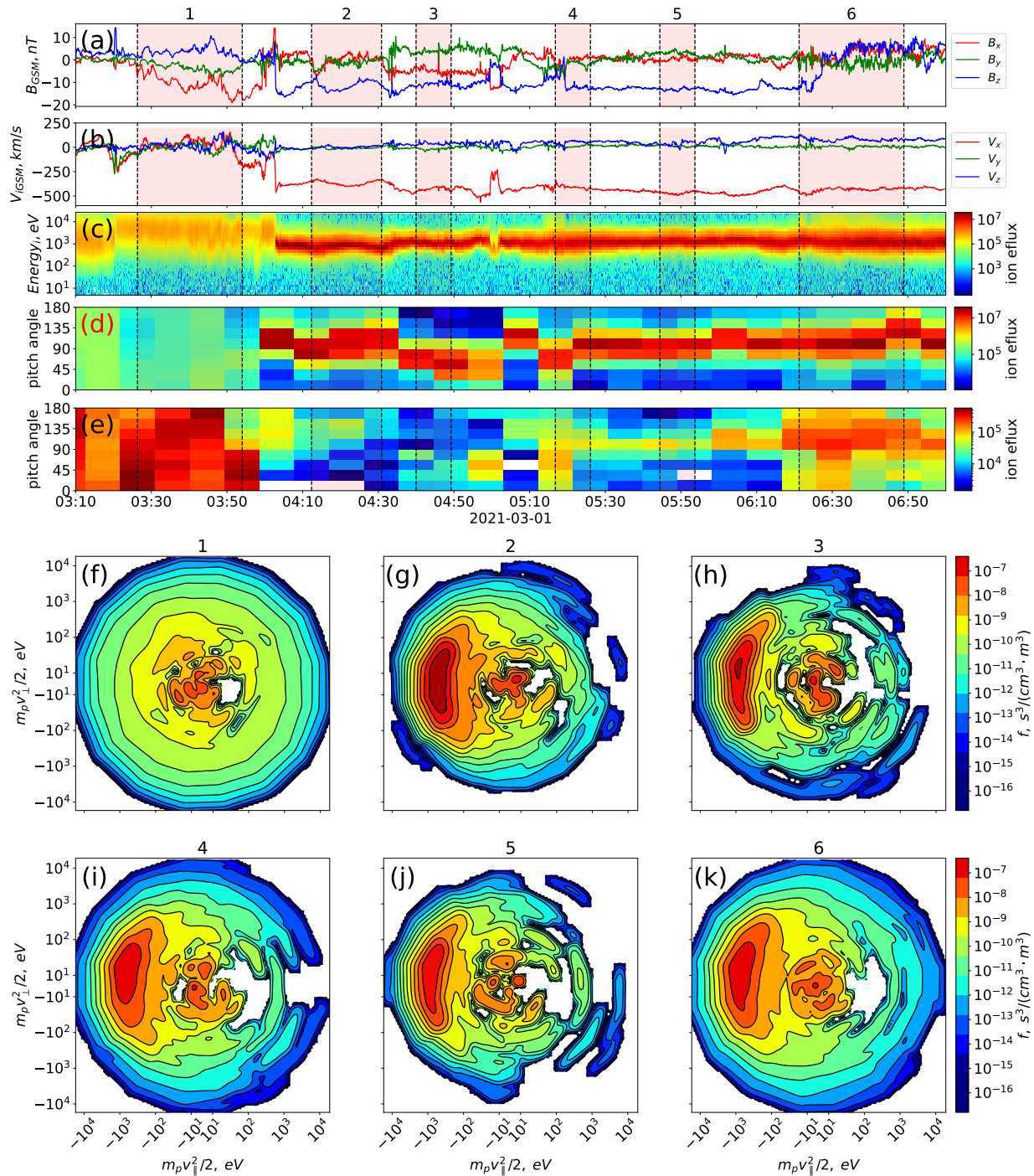


**Figure 5.** The overview of the solar wind discontinuity interaction with the magnetopause (THEMIS B): magnetic field components (a), ion flow components (b), ion energy spectrum (c), ion pitch-angle distributions for different energy ranges ([100 – 2000] eV for (d) and [4 – 20] keV for (e)), 2D cuts of ion distributions in  $(m_p v_{\perp}^2/2, m_p v_{\parallel}^2/2)$  plane for several intervals indicated by numbers.

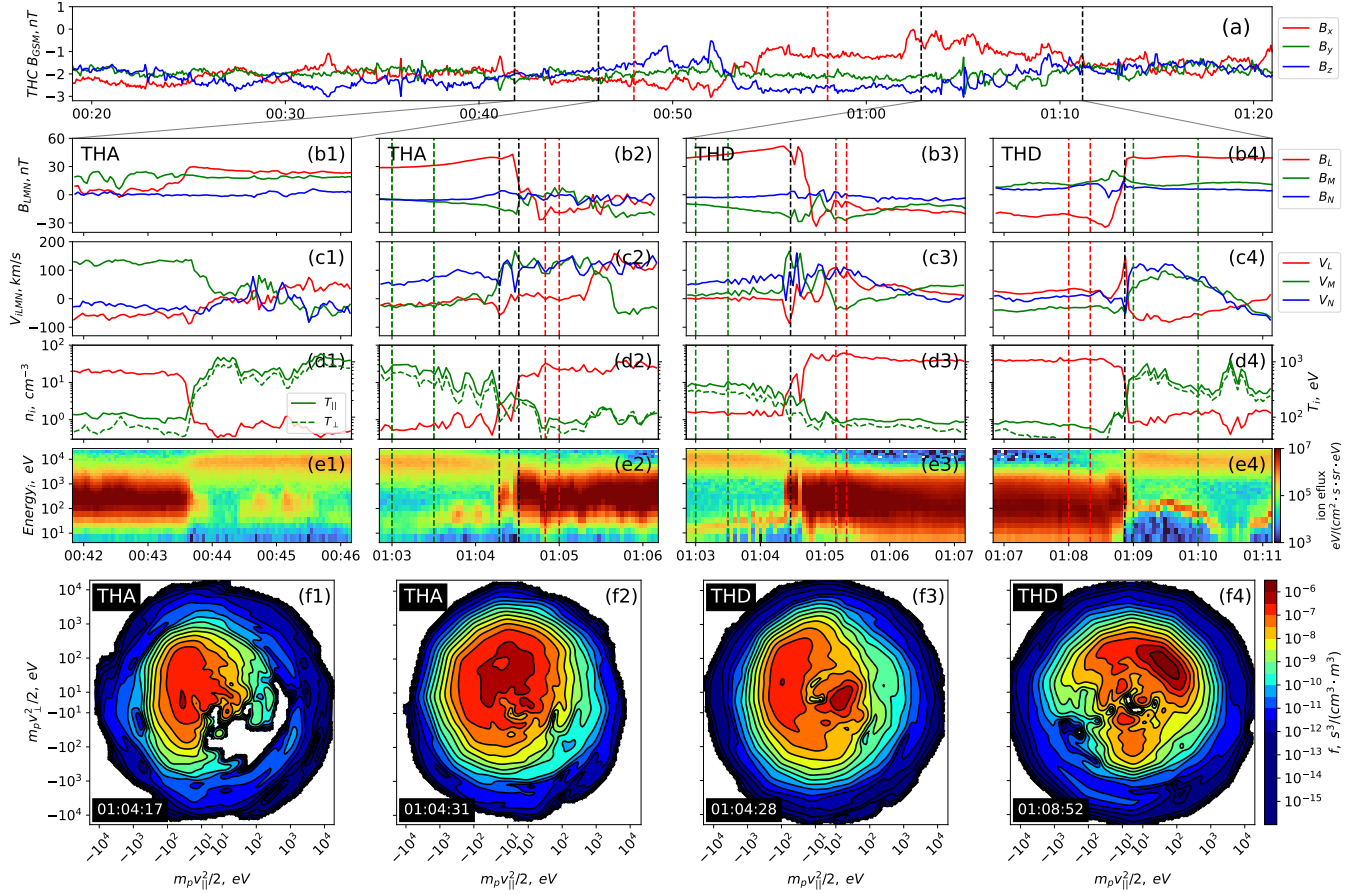


**Figure 6.** Overview of THEMIS&ARTEMIS observations on 2019-09-20. From top to bottom: (a) solar wind discontinuity shown by two red dashed lines (magnetic field at ARTEMIS#2); magnetic field of the magnetopause crossings by THEMIS A and D before (b1) and after (b2-b4) the solar wind discontinuity impact; plasma flow velocities (c), plasma density and ion temperature (d), ion spectra (e) for the magnetopause crossings before (1) and after (2-4) the solar wind discontinuity impact; the corresponding ion velocity distributions around the magnetopause (f1-f4).

#### 2.4. Supporting events

Events in Figs. 2, 4 demonstrate the magnetopause reconnection after the solar wind discontinuity impact, but for these events we do not have observations of the non-reconnected magnetopause before the arrival of the discontinuity. Thus, the reconnection might have already started even before the discontinuity arrives, and would be only modified by this impact. To verify the key role of the discontinuity impact in triggering the reconnection, we analyze three supporting events when the spacecraft crossed the magnetopause before and after the discontinuity arrives. In all three events the magnetopause does not show reconnection signatures before the discontinuity impact, but becomes reconnected only afterwards.

Figure 6 shows an overview of the 2019-09-20 event. THEMIS C is at  $r_{GSM} \sim (-24, -57, 12) R_E$  and observes a series of discontinuities at  $\sim 00:48-00:55$  UT. During 00:20-01:20 UT, THEMIS A crosses the magnetopause several times, and two such crossings are shown in panels (b1-e1) and (b2-e2). As shown in the figure, during the first crossing before the discontinuity arrives at the magnetopause,

there are no ion jets or other signatures of the reconnection, i.e., THEMIS A crosses non-reconnected magnetopause.

In the second crossing right after the discontinuity arrives at the magnetopause, THEMIS A is at  $r_{GSM} \sim (9, 9, 2)R_E$  and observes the bifurcated current sheet with several ion jets, the primary signatures of the magnetic reconnection. In the local coordinate system, the observed ion bulk velocity change across the magnetopause at two times, as marked by the black dashed lines in panels (b2-e2), are  $\Delta v_{1obs} \sim (-56, -34, -79)$  km/s and  $\Delta v_{2obs} \sim (5, 25, -65)$  km/s. Magnitudes of these velocities, however, are much smaller than magnitudes of velocity changes estimated from the model of the reconnected magnetopause [Phan et al. \(2013\)](#); [Hudson \(1970\)](#); [Paschmann et al. \(1986\)](#):

$$\Delta \mathbf{v}_{pred} = \mathbf{v}_2 - \mathbf{v}_1 = \pm \sqrt{\frac{1 - \alpha_1}{4\pi\rho_i}} (\mathbf{B}_2(1 - \alpha_2)/(1 - \alpha_1) - \mathbf{B}_1)$$

where  $\alpha = \frac{4\pi(p_{\parallel} - p_{\perp})}{B^2}$  is the anisotropy factor,  $p_{\parallel}$ ,  $p_{\perp}$  are the plasma pressures parallel and perpendicular to  $\mathbf{B}$ . Subscripts 1 and 2 denote the magnetosheath inflow region (marked by red dashed lines in Fig. 6(b-e)) and the jet region, respectively. For this crossing,  $\Delta v_{1pred} \sim (-250, 81, -16)$  km/s and  $\Delta v_{2pred} \sim (230, -107, 3)$  km/s. Moreover, the observed velocity changes are also smaller than the estimate of the asymmetric Alfvén velocity,  $V_{Al,asym} \sim 133.05$  km/s. Therefore, despite that quasi-parallel ion flows are observed in the ion velocity distribution (see panels (f1-f2)), the observed and predicted values of ion velocity changes are much different, and THEMIS A may not observe the reconnected magnetopause.

After the discontinuity arrives at the magnetopause, both THEMIS D and THEMIS E (not shown) observe almost the same signatures of magnetic reconnection, though much more evident at THEMIS D. Both spacecraft are in the magnetosphere near the magnetopause at  $r_{dGSM} \sim (9, 7, 1)R_E$  and  $r_{eGSM} \sim (5, 12, 1)R_E$ , and due to the magnetosphere compression by the discontinuity both spacecraft appear in the magnetosheath after the discontinuity (panels (b3-e3)). The estimated magnetopause thickness for the two crossings shown in panels (b3-e3) and (b4-e4) are  $L_{d1} \sim 924$  km ( $\sim 2.38\rho_{iMSH}$ , where  $\rho_{iMSH} = \frac{m_i c v T}{e B}$  is the averaged value of the ion thermal gyroradius in the magnetosheath) and  $L_{d1} \sim 821$  km ( $\sim 2.26\rho_{iMSH}$ ) (see detailed description of the method in [Haaland et al. 2014](#)). Therefore, THEMIS D indeed crosses a ion-scale magnetopause current sheet. In the local coordinate system, the observed and predicted ion velocity changes across the magnetopause (at the two times marked by the black dashed lines in panels (b3-e3) and (b4-e4)) are  $\Delta v_{1obs} \sim (-175, 200, -9)$  km/s,  $\Delta v_{1pred} \sim (-173, -1, 6)$  km/s and  $\Delta v_{2obs} \sim (115, -21, -59)$  km/s,  $\Delta v_{2pred} \sim (167, 7, -12)$  km/s. The estimated asymmetric Alfvén velocity is  $V_{Al,asym} \sim 124.88$  km/s. Moreover, quasi-parallel flows are seen in the ion velocity distribution (panel (f3)) during the first THEMIS D crossing. During the second THEMIS D crossing, the strong ion jet is tangential to the magnetopause, but at the moment of the jet observation the main magnetic field component is around zero, i.e., there is a large uncertainty in projecting to the local magnetic field direction. During both crossings, the nonzero normal velocity components are observed together with the low energy population (panels (e3-e4)). Therefore, THEMIS D observations clearly demonstrate the magnetopause reconnection after the discontinuity impact, whereas THEMIS A observations confirm that the magnetopause was not reconnected before this impact.

Figure 7 shows another example of the solar wind discontinuity interaction with the magnetopause on 2016-07-28. During this event, THEMIS C is in the solar wind at  $r_{GSM} \sim (20, -52, 16)R_E$

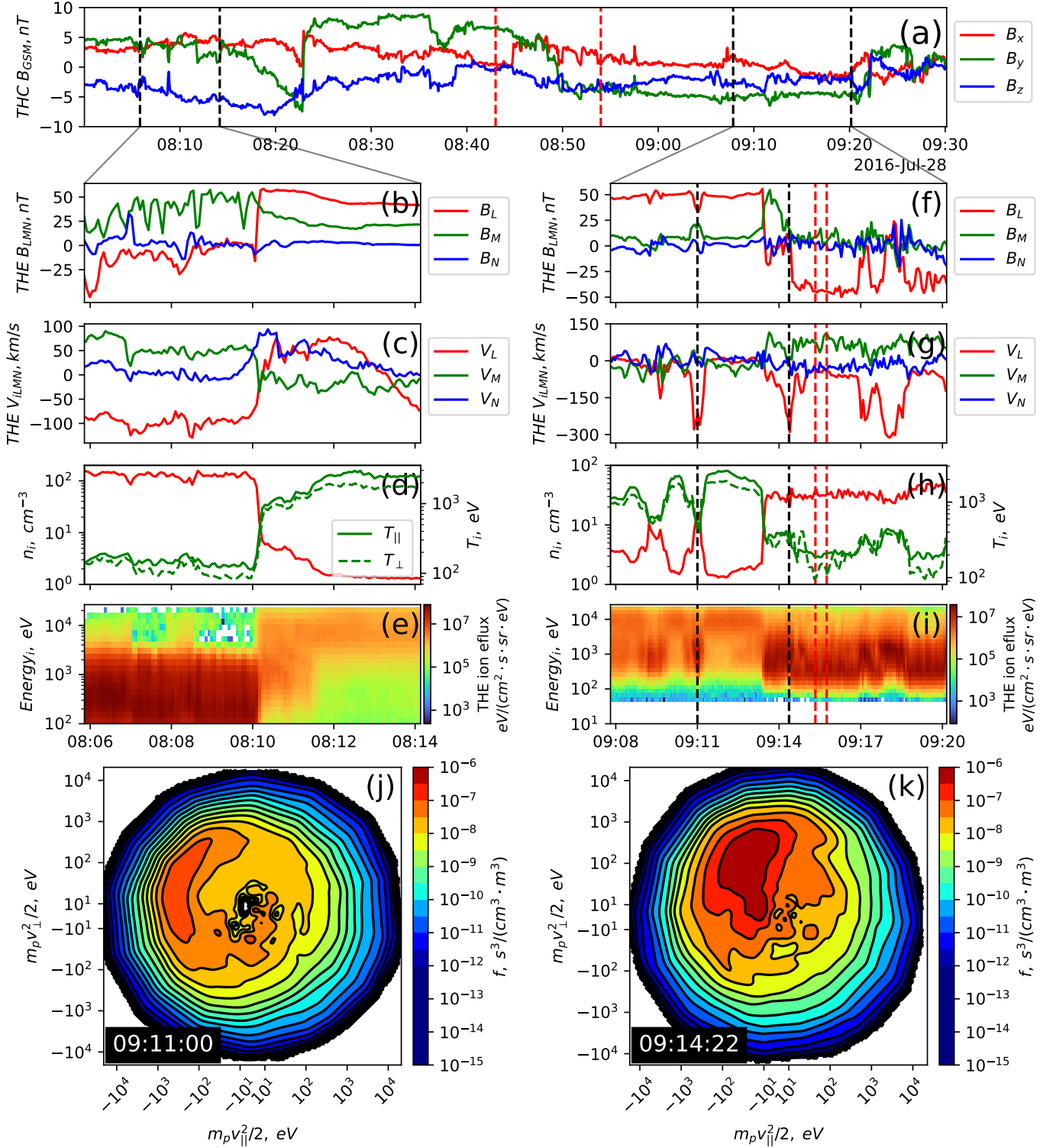


**Figure 7.** Overview of THEMIS&ARTEMIS observations on 2016-07-28. From top to bottom: (a) solar wind discontinuity as marked by the two red dashed lines (magnetic field at ARTEMIS#2); magnetic field of the magnetopause crossings by THEMIS E before (b) and after (f) the solar wind discontinuity impact; plasma flow velocities (c and g), plasma density and ion temperature (d and h), ion spectra (e and i) for the magnetopause crossings from (b and f); ion velocity distributions around the magnetopause crossing after the solar wind discontinuity impact (j,k).

and observes a series of discontinuities at  $\sim 08:43-08:54$  UT. The same series of discontinuities are observed by THEMIS D in the magnetosheath around  $09:00-09:05$  UT (not shown). Within  $08:06-09:30$  UT, THEMIS A crosses the magnetopause twice. The first crossing is shown in panels (b-e), and for this crossing the observed and predicted flow changes are  $\Delta v_{obs} \sim (163, -58, 91)$  km/s and  $\Delta v_{pred} \sim (100, 1047, -14)$  km/s, whereas the estimated asymmetric Alfvén velocity is  $V_{Al,asym} \sim 16$  km/s. The large difference in the observed and predicted ion velocity change indicates that THEMIS A crosses the non-reconnected magnetopause.

Panels (f-i) show the second crossing, after the discontinuity arrives to the magnetopause. Starting from  $09:00$  UT (when the discontinuity is detected in the magnetosheath by THEMIS D), THEMIS A observes variations in the magnetospheric magnetic field, whereas during the magnetopause crossing THEMIS A detects the bifurcated current sheet and several ion jets (the primary signatures of the magnetic reconnection). The observed and estimated ion velocity changes for the two times marked by black dashed lines in panels (f-i) are  $\Delta v_{1obs} \sim (-206, -63, 22)$  km/s,  $\Delta v_{1pred} \sim (-332, -31, -11)$  km/s and  $\Delta v_{2obs} \sim (-251, -53, 10)$  km/s,  $\Delta v_{2pred} \sim (-211, 1, 2)$  km/s. The estimated asymmetric Alfvén velocity is  $V_{Al,asym} \sim 236.73$  km/s. Therefore, the similar velocity change between observations and the model prediction suggests that THEMIS A indeed crosses the reconnected magnetopause. Moreover, panels (j-k) show the corresponding 2D slices of the ion distribution functions with clear quasi-parallel ion jets. Thus, these observations show that the interaction between the solar wind discontinuity and the magnetopause can trigger magnetic reconnection of the initially non-reconnected magnetopause.

The third supplementary event is shown in Figure 8. During this event, THEMIS C is in the solar wind at  $r_{GSM} \sim (28, -51, 15)R_E$  and observes a series of discontinuities during  $\sim 11:33-11:43$  UT. The same series of discontinuities are observed by THEMIS A in the magnetosheath around  $\sim 11:30$  UT (not shown). Within  $11:10-12:20$  UT, THEMIS E crosses the magnetopause several times. The first and the second crossings are shown in panels (b-e). During these crossings, no ion jets or other reconnection signatures are detected. Panels (f-i) show the third crossing, after the discontinuity arrives at the magnetopause. During the magnetopause crossing, THEMIS E is at  $r_{GSM} \sim (11, -4, 5)R_E$  and observes variations in the magnetic field accompanied by ion jets. The observed and estimated ion velocity changes for the two times marked by black dashed lines in panels (f-i) are  $\Delta v_{1obs} \sim (204, -82, -41)$  km/s,  $\Delta v_{1pred} \sim (225, 61, -20)$  km/s and  $\Delta v_{2obs} \sim (238, -29, -2)$  km/s,  $\Delta v_{2pred} \sim (251, 16, -25)$  km/s. The estimated asymmetric Alfvén velocity is  $V_{Al,asym} \sim 173$  km/s. Panels (j-k) show the corresponding 2D slices of the ion distribution functions with quasi-parallel ion jets. As in events from Figs. 6, 7, the observed ion velocity changes are comparable to the predicted changes and to the value of the asymmetric Alfvén velocity, whereas ion velocity distributions show clear field-aligned ion jets. Therefore, Fig. 8 confirms results from Figs. 6, 7 that the solar wind discontinuity impact may trigger the reconnection of the initially non-reconnected magnetopause.

### 3. GLOBAL HYBRID SIMULATION

In this section, a 3-D global hybrid code of Lin & Wang (2005); Tan et al. (2011); Guo et al. (2018, 2020) is applied to investigate the evolution of the solar wind discontinuity and understand the dayside magnetopause reconnection driven by the impact of the discontinuity. In this hybrid model, ions are considered as fully kinetic particles, while electrons are taken to be a massless fluid. A spherical coordinate system  $(r, \theta, \phi)$  is employed. The simulation domain covers the dayside region ( $x \geq 0$ )

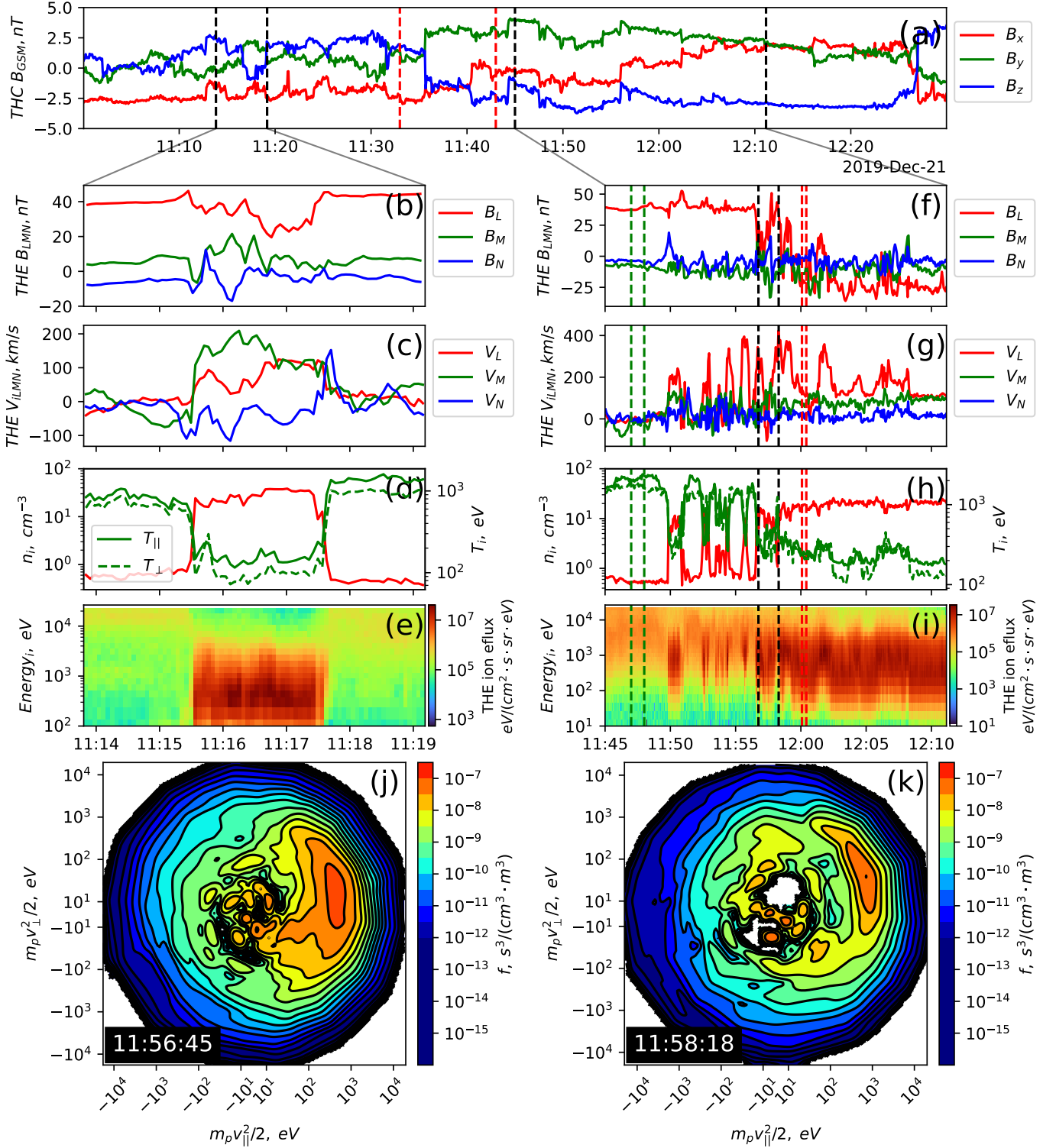


**Figure 8.** Overview of THEMIS&ARTEMIS observations on 2019-12-21. From top to bottom: (a) solar wind discontinuity shown by two red dashed lines (magnetic field at ARTEMIS#2); magnetic field of the magnetopause crossings by THEMIS E before (b) and after (f) the solar wind discontinuity impact; plasma flow velocities (c and g), plasma density and ion temperature (d and h), ion spectra (e and i) for the magnetopause crossings from (b and f); ion velocity distributions around the magnetopause crossing after the solar wind discontinuity impact (j,k).



with  $r \in [3.5R_E, 25R_E]$ , where  $R_E$  is the Earth radius. A perfectly conducting boundary condition is applied for the inner boundary at  $r = 3.5R_E$ . The inflow boundary is located at  $r = 20R_E$ , where the solar wind flows toward the Earth together with the interplanetary magnetic field (IMF). The initial IMF is assumed to be  $(-1.25, -3.96, -3.86)$  nT, the solar wind ion number density is set as  $N_0 = 12.0\text{cm}^{-3}$ , and the ion temperature is chosen as 6.7eV, based on the conditions observed by THEMIS C before the rotational discontinuity arrives (the first, day-side event). The IMF on the sunward side of the discontinuity is chosen as  $(-0.24, -5.45, 1.52)$  nT. The solar wind velocity changes across the rotational discontinuity from  $(-356.4, -27.2, -3.87)$  km/s to  $(-350.0, 17.7, -30.37)$  km/s. More detailed descriptions of how to impose discontinuity in the hybrid model can be found elsewhere (Guo et al. 2018, 2021a). The number of grid cells is  $n_r \times n_\theta \times n_\phi = 320 \times 220 \times 180$ , and a total of  $\sim 5 \times 10^9$  particles are used. To reduce computing expenses, the grid cells in the radial direction are set to be non-uniform. A smaller grid size of  $\Delta r \simeq 0.025 \rightarrow 0.05R_E$  is used around the magnetopause and in the magnetosheath, while a larger grid size is set in the solar wind. We also set the solar wind ion inertial length equal to  $0.1R_E$ , i.e., a scaling factor is about  $\sim 9.57$  is needed to scale the time and velocities to the realistic values.

Figure 9 shows the discontinuity in the numerical simulation at three time intervals. The initial solar wind discontinuity (left panels) repeats the configuration and magnetic field components of the ARTEMIS observations from Fig. 2, a rotational discontinuity with a constant plasma density and jumps of plasma velocity across the discontinuity. The discontinuity downstream of the bow shock (center panels) is characterized by a magnetic field increase from the initial  $\sim 5$  nT to  $\sim 20$  nT. This magnetic field compression resembles the THEMIS A observations in the magnetosheath (see Fig. 2). In the magnetosheath, the ion number density  $N_i$  (Fig. 9c2) and ion temperature  $T_i$  (Fig. 9d2) increase, and the ion flow brakes with the ion bulk velocity  $V_i$  (Fig. 9b2) slows down. When the discontinuity arrives at the magnetopause (right panels), the simulation shows typical signatures of magnetic reconnection: plasma jet in  $V_z$  (Fig. 9b3) and an increase of ion temperature (Fig. 9d3) due to magnetospheric plasma leakage (compare with THEMIS A observations shown in Fig. 3).

To further confirm that the discontinuity interaction with the magnetopause triggers magnetic reconnection, we visualize the solar wind discontinuity motion. The contour plots of Figure 10 show the magnetic field strength for three moments of time: before arriving the solar wind discontinuity (top panels), when solar wind discontinuity interacts with the magnetopause (middle panels), and when solar wind discontinuity passes through the magnetopause (bottom panels). In the figure, the orange lines mark the magnetic field lines outside the magnetopause, and the black lines denote the field lines at the magnetopause. At  $t = 20$ , before the solar wind discontinuity arrives at the magnetopause, magnetopause flux ropes has formed by reconnection between the initial IMF  $(-1.25, -3.96, -3.86)$  nT and the dipole field, which are denoted by the black field lines. It is found that the magnetopause reconnection occurs in the high-latitude regions of the dayside magnetopause on the dawnside and duskside, which is marked by the blue boxes (note this region were not observed by spacecraft). When the solar wind discontinuity interacts with the magnetopause, at  $t = 30$ , magnetic reconnection is seen at low- and middle latitudes of the dayside magnetopause, which is denoted as the red box. Finally, when the solar wind discontinuity passes through the magnetopause, no reconnection is found at the dayside magnetopause due to the magnetic field turns from  $(-1.25, -3.96, -3.86)$  nT to  $(-0.14, -5.45, 1.52)$  nT.

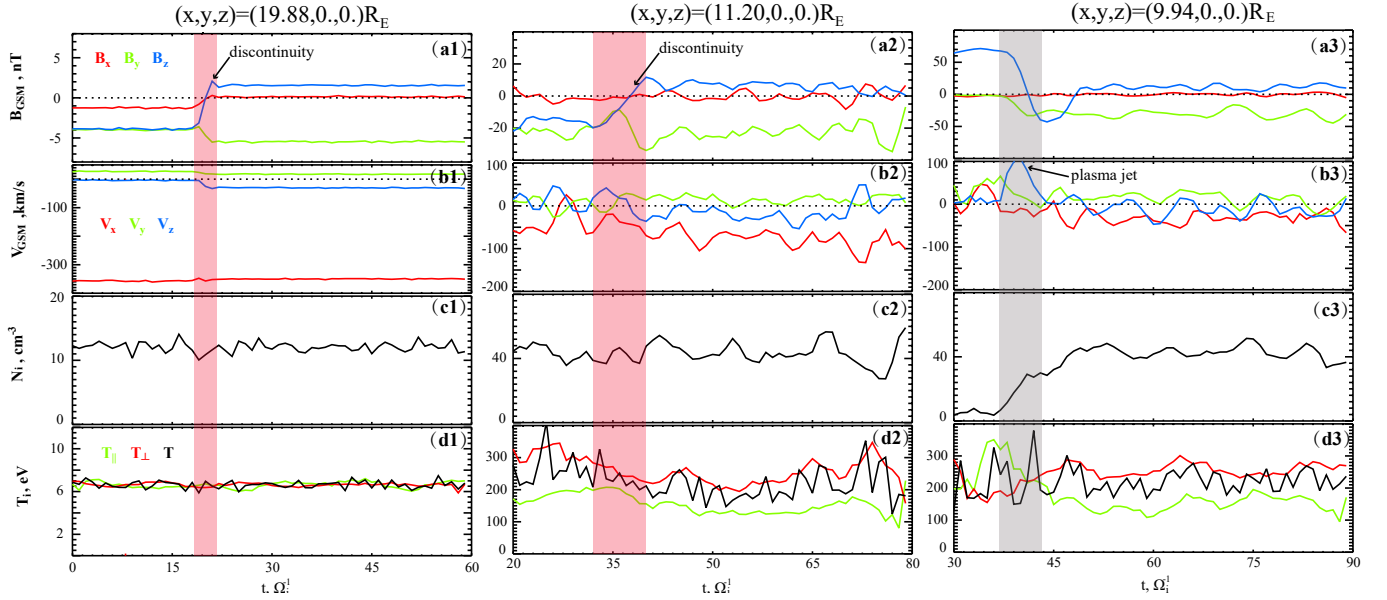


**Figure 9.** The overview of global hybrid simulation of solar wind discontinuity (left panels), the same discontinuity in the downstream of the bow shock (center panels), and magnetopause reconnection (right panels): magnetic field vector (a1-a3), ion velocity components (b1-b3), ion number density (c1-c3), and ion temperature (d1-d3).

Using advantage of the hybrid simulation which treats ions as particles, we plot ion distribution functions right around the region of the magnetopause impact by the solar wind discontinuity. Figure 11 shows that distributions on the magnetosphere side contain two ion populations: the hot field-aligned flowing population and cold population. The latter one penetrates from the magnetosheath along reconnected magnetic field lines. These model distributions resemble observational distributions #3,5 from Fig. 3, which are measured when cold magnetosheath plasma injections are observed within the magnetosphere. Therefore, simulation results shown in Fig. 9-11 confirm the scenario of the magnetic reconnection driven by the magnetopause impact by solar wind discontinuity.

#### 4. DISCUSSION AND CONCLUSIONS

We presented observational and simulation evidence that the solar wind discontinuity impact may trigger the magnetic reconnection at the magnetopause. More general, the rotational discontinuity is intensified by crossing the shock wave (the Earth bow shock) and then impacts the tangential discontinuity (magnetopause), triggering the magnetic reconnection and plasma mixing (cross-penetration of magnetosheath and magnetospheric plasmas). We note that the rotational discontinuity interaction with the bow shock significantly modifies the discontinuity properties and add compressional perturbations, and thus we shall rather discuss interaction of the tangential discontinuity (magnetopause) with the discontinuity sharing properties of both rotational and tangential discontinuities. Reconnection of such rotational discontinuity downstream of the bow shock is possible when the bow shock is quasi-parallel (Guo et al. 2021a) or quasi-perpendicular, with large magnetic field rotation

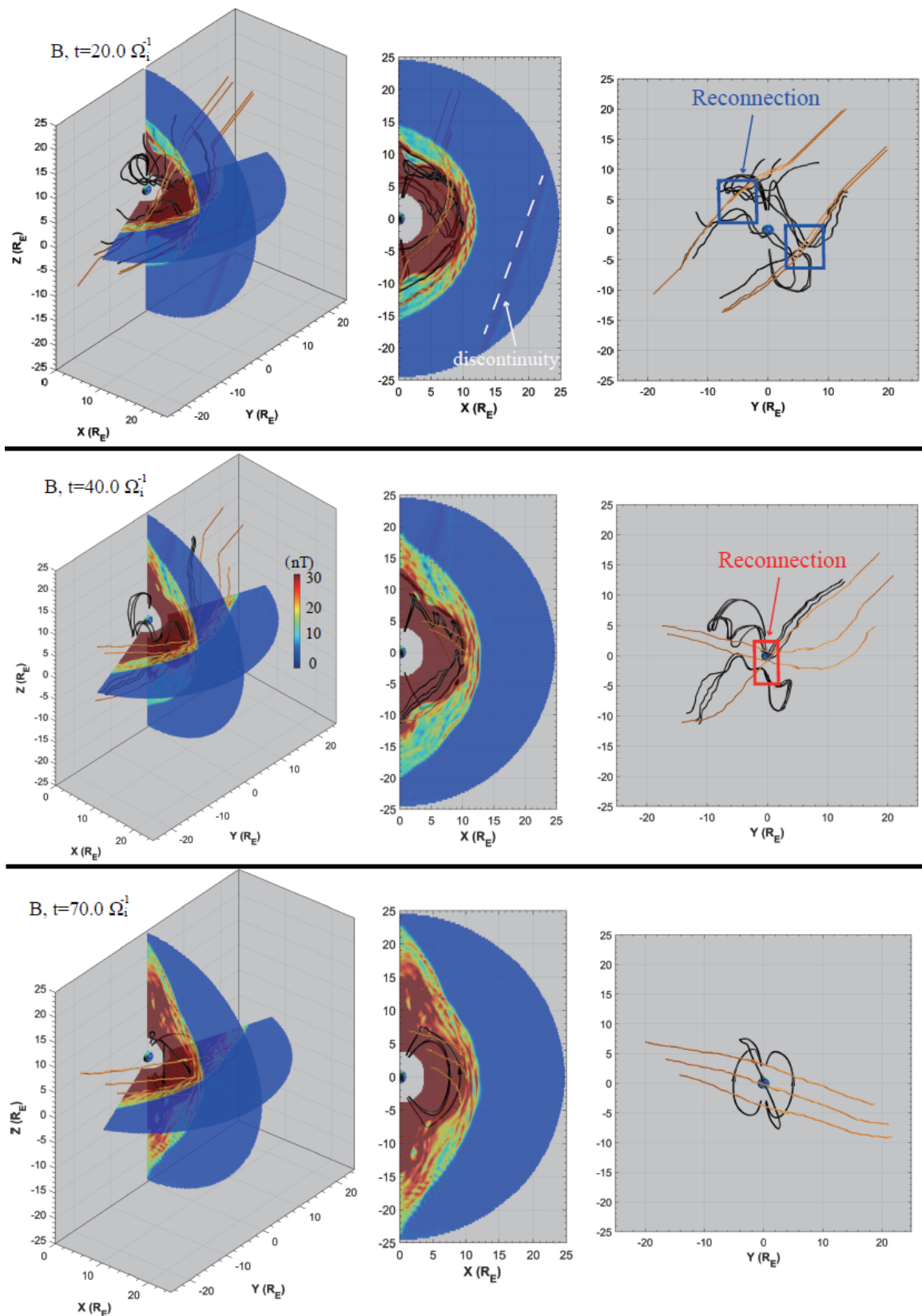


**Figure 10.** The overview of solar wind discontinuity interaction with the magnetosphere: magnetic field strength in 3D and 2D planes. Three moments are shown: at  $t \sim 20\Omega_i^{-1}$  the RD was in the solar wind, at  $t \sim 40\Omega_i^{-1}$  the RD interacts with the magnetopause, at  $t \sim 70\Omega_i^{-1}$  the RD passes through the magnetopause.

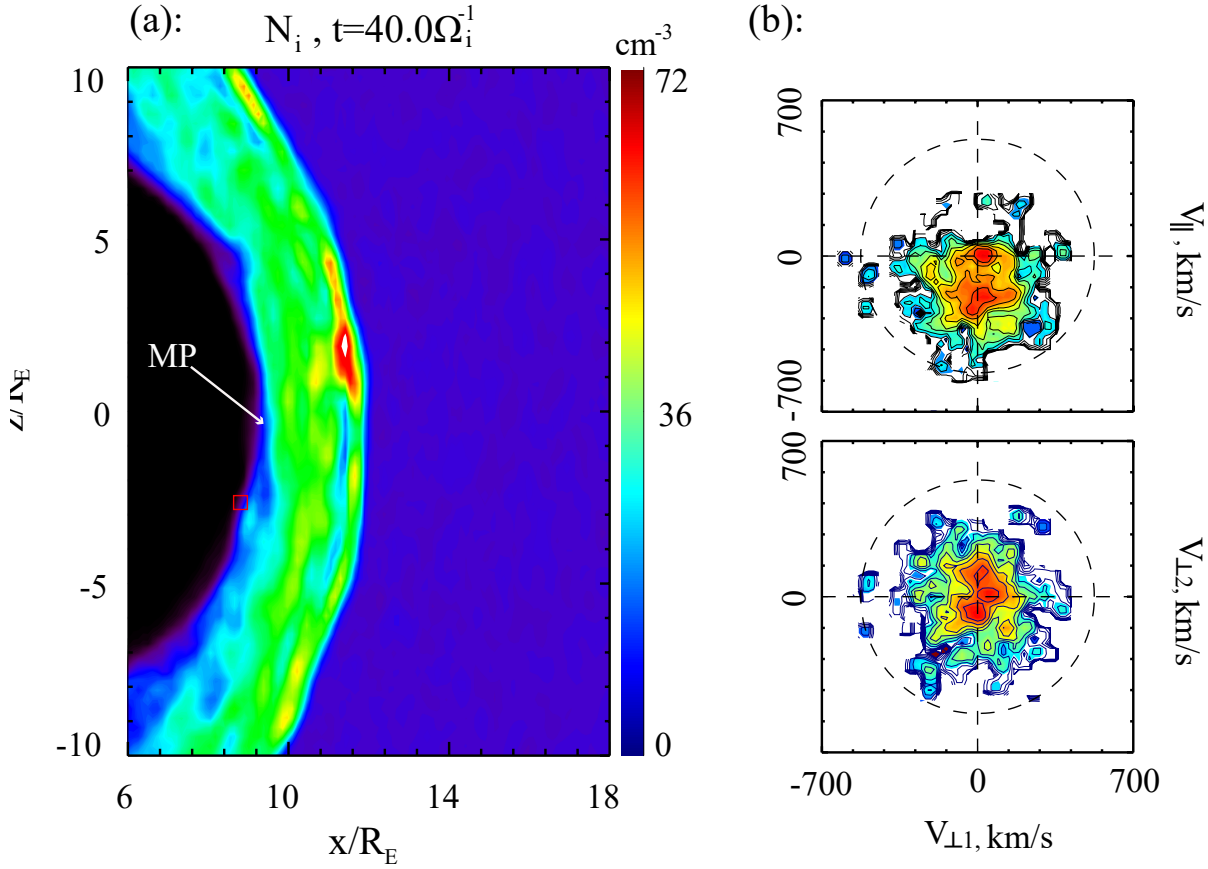


**Figure 11.** (a) A zoom-in view of the ion number density in the  $y=0$  plane; (b) Ion velocity distributions in the  $(V_{\perp,1}, v_{\parallel})$  and  $(V_{\perp,1}, V_{\perp,2})$  planes on the magnetosphere side at the location marked by the red box in Fig. 8a.

angle (Guo et al. 2021b). In our cases, the bow shock configuration does not support the discontinuity reconnection in the magnetosheath, and thus discontinuity reaches the magnetopause and triggers the magnetopause reconnection. Although this scenario has been considered for the specific plasma system of the solar wind interaction with the Earth’s magnetosphere, we may speculate about an application of the similar discontinuity-discontinuity interaction in other systems.

Discontinuity interactions should be rather common phenomena for solar wind (and more general, stellar wind) where such discontinuities may be formed by Alfvén wave turbulence (e.g., Buti et al. 1998; Vasquez & Hollweg 1999, 2001) and nonlinear Alfvén wave steepening (Hada et al. 1989; Kennel et al. 1988; Malkov et al. 1991; Medvedev et al. 1997), and then are transported by plasma flows having spatially and temporally varying flow speed and Alfvén speed. Such variations of plasma flow speed and Alfvén speed would force discontinuity-discontinuity interactions, with the possible triggering of the magnetic reconnection and plasma mixing. This scenario is actively discussed for the solar wind turbulence (see, e.g., in Greco et al. 2008, 2009; Servidio et al. 2011a,b; Pecora et al.

2018; Vörös et al. 2021), and it can be quite perspective for magnetized flows of pulsar wind carrying multiple discontinuities (e.g., Coroniti 1990; Bogovalov 1999; Spitkovsky 2006; Cerutti & Giacinti 2020). For pulsar wind the magnetic reconnection is considered as an important mechanism of magnetic energy transformation to plasma energy with the magnetic field reduction and formation of pulsar flares (Arons 2012; Abdo et al. 2011; Aharonian et al. 2012). However, only internal instabilities of discontinuities and their interaction with the shock waves have been considered as a trigger of the magnetic reconnection (e.g., Lyubarsky & Kirk 2001; Uzdensky et al. 2011; Cerutti et al. 2012; Cerutti & Philippov 2017). A proposed here discontinuity-discontinuity interaction may be an alternative mechanism for the magnetic reconnection triggering, that would work for generally stable rotational discontinuities and would not require magnetic reconnection localization around the shock wave.

To conclude, we have described the magnetic reconnection triggering due to the interaction of two discontinuities: the solar wind rotational discontinuity (modified and intensified via the bow shock crossing) and tangential discontinuity of the Earth’s magnetopause. Spacecraft observations and global hybrid simulations demonstrate that magnetic reconnection triggered by the solar discontinuity impact on the magnetopause results in mixing of hot rarefied magnetospheric plasma and cold dense solar wind (magnetosheath) plasma. We also show that such discontinuity-driven reconnection can be observed at both day-side magnetopause (where solar wind plasma flow contributes significantly to the pressure balance across the magnetopause) and the deep flank magnetopause (where solar wind plasma flow is almost tangential to the magnetopause surface). These results underline an importance of discontinuity-discontinuity interactions for plasma mixing via magnetic field line reconnection.

#### ACKNOWLEDGEMENTS

Alexander Lukin and Anatoli Petrukovich acknowledge support from Russian Science Foundation through grant No. 19-12-00313 covering the covering general spacecraft data analysis and data/model comparison parts of this work. Anton Artemyev acknowledges support from NASA HSR 80NSSC20K1788 and HGI 80NSSC22K0752 covering analysis of discontinuity configuration aspect of this work.

Anton Artemyev and Xiaojia Zhang also acknowledge NASA contract NAS5-02099 for use of data from the THEMIS mission. We thank K. H. Glassmeier, U. Auster, and W. Baumjohann for the use of FGM data provided under the lead of the Technical University of Braunschweig and with financial support through the German Ministry for Economy and Technology and the German Aerospace Center (DLR) under contract 50 OC 0302. THEMIS data is available at <http://themis.ssl.berkeley.edu>. Data access and processing was done using SPEDAS V4.1 (Angelopoulos et al. 2019) available at <https://spedas.org/>.

#### REFERENCES

- |  |  |
|--|--|
| Abdo, A. A., Ackermann, M., Ajello, M., et al. 2011, <i>Science</i> , 331, 739, doi: <a href="https://doi.org/10.1126/science.1199705">10.1126/science.1199705</a> | An, X., Liu, T. Z., Bortnik, J., Osmane, A., & Angelopoulos, V. 2020, <i>ApJ</i> , 901, 73, doi: <a href="https://doi.org/10.3847/1538-4357/abaf03">10.3847/1538-4357/abaf03</a> |
| Aharonian, F. A., Bogovalov, S. V., & Khangulyan, D. 2012, <i>Nature</i> , 482, 507, doi: <a href="https://doi.org/10.1038/nature10793">10.1038/nature10793</a>    | Angelopoulos, V. 2008, <i>SSRv</i> , 141, 5, doi: <a href="https://doi.org/10.1007/s11214-008-9336-1">10.1007/s11214-008-9336-1</a>  |
|  | —. 2011, <i>SSRv</i> , 165, 3, doi: <a href="https://doi.org/10.1007/s11214-010-9687-2">10.1007/s11214-010-9687-2</a>  |

- Angelopoulos, V., Cruce, P., Drozdov, A., et al. 2019, *SSRv*, 215, 9, doi: [10.1007/s11214-018-0576-4](https://doi.org/10.1007/s11214-018-0576-4)
- Archer, M. O., Horbury, T. S., & Eastwood, J. P. 2012, *Journal of Geophysical Research*, 117, A05228, doi: [10.1029/2011JA017468](https://doi.org/10.1029/2011JA017468)
- Archer, M. O., Turner, D. L., Eastwood, J. P., Horbury, T. S., & Schwartz, S. J. 2014, *Journal of Geophysical Research (Space Physics)*, 119, 8117, doi: [10.1002/2014JA020342](https://doi.org/10.1002/2014JA020342)
- Archer, M. O., Turner, D. L., Eastwood, J. P., Schwartz, S. J., & Horbury, T. S. 2015, *Planet. Space Sci.*, 106, 56, doi: [10.1016/j.pss.2014.11.026](https://doi.org/10.1016/j.pss.2014.11.026)
- Arons, J. 2012, *SSRv*, 173, 341, doi: [10.1007/s11214-012-9885-1](https://doi.org/10.1007/s11214-012-9885-1)
- Artemyev, A. V., Angelopoulos, V., Halekas, J. S., et al. 2018, *ApJ*, 859, 95, doi: [10.3847/1538-4357/aabe89](https://doi.org/10.3847/1538-4357/aabe89)
- Artemyev, A. V., Angelopoulos, V., & Vasko, I. Y. 2019, *Journal of Geophysical Research (Space Physics)*, 124, 3858, doi: [10.1029/2019JA026597](https://doi.org/10.1029/2019JA026597)
- Auster, H. U., Glassmeier, K. H., Magnes, W., et al. 2008, *SSRv*, 141, 235, doi: [10.1007/s11214-008-9365-9](https://doi.org/10.1007/s11214-008-9365-9)
- Birn, J., & Priest, E. R. 2007, *Reconnection of magnetic fields : magnetohydrodynamics and collisionless theory and observations*, ed. Birn, J. & Priest, E. R.
- Bogovalov, S. V. 1999, *Astronomy and Astrophysics*, 349, 1017
- Burch, J. L., Moore, T. E., Torbert, R. B., & Giles, B. L. 2016, *SSRv*, 199, 5, doi: [10.1007/s11214-015-0164-9](https://doi.org/10.1007/s11214-015-0164-9)
- Burch, J. L., Torbert, R. B., Phan, T. D., et al. 2016, *Science*, doi: [10.1126/science.aaf2939](https://doi.org/10.1126/science.aaf2939)
- Buti, B., Jayanti, V., Viñas, A. F., et al. 1998, *Geophys. Res. Lett.*, 25, 2377, doi: [10.1029/98GL01688](https://doi.org/10.1029/98GL01688)
- Cable, S., & Lin, Y. 1998, *J. Geophys. Res.*, 103, 29551, doi: [10.1029/1998JA900025](https://doi.org/10.1029/1998JA900025)
- Cassak, P., & Shay, M. 2007, *Physics of Plasmas*, 14, 102114
- Cerutti, B., & Giacinti, G. 2020, *A&A*, 642, A123, doi: [10.1051/0004-6361/202038883](https://doi.org/10.1051/0004-6361/202038883)
- Cerutti, B., & Philippov, A. A. 2017, *A&A*, 607, A134, doi: [10.1051/0004-6361/201731680](https://doi.org/10.1051/0004-6361/201731680)
- Cerutti, B., Uzdensky, D. A., & Begelman, M. C. 2012, *ApJ*, 746, 148, doi: [10.1088/0004-637X/746/2/148](https://doi.org/10.1088/0004-637X/746/2/148)
- Chen, L.-J., Ng, J., Omelchenko, Y., & Wang, S. 2021, *Geophys. Res. Lett.*, 48, e93029, doi: [10.1029/2021GL093029](https://doi.org/10.1029/2021GL093029)
- Coroniti, F. V. 1990, *ApJ*, 349, 538, doi: [10.1086/168340](https://doi.org/10.1086/168340)
- De Keyser, J., Dunlop, M. W., Owen, C. J., et al. 2005, *SSRv*, 118, 231, doi: [10.1007/s11214-005-3834-1](https://doi.org/10.1007/s11214-005-3834-1)
- Farrugia, C. J., Vasquez, B., Richardson, I. G., et al. 2001, *Advances in Space Research*, 28, 759, doi: [10.1016/S0273-1177\(01\)00529-4](https://doi.org/10.1016/S0273-1177(01)00529-4)
- Farrugia, C. J., Cohen, I. J., Vasquez, B. J., et al. 2018, *Journal of Geophysical Research (Space Physics)*, 123, 8983, doi: [10.1029/2018GL081804](https://doi.org/10.1029/2018GL081804)
- Gary, S., Winske, D., McKean, M. E., et al. 1995, *Washington DC American Geophysical Union Geophysical Monograph Series*, 90, 123, doi: [10.1029/GM090p0123](https://doi.org/10.1029/GM090p0123)
- Gingell, I., Schwartz, S. J., Eastwood, J. P., et al. 2019, *Geophys. Res. Lett.*, 46, 1177, doi: [10.1029/2018GL081804](https://doi.org/10.1029/2018GL081804)
- . 2020, *Journal of Geophysical Research (Space Physics)*, 125, e27119, doi: [10.1029/2019JA027119](https://doi.org/10.1029/2019JA027119)
- Gonzalez, W., & Parker, E. 2016, *Magnetic Reconnection*, Vol. 427, doi: [10.1007/978-3-319-26432-5](https://doi.org/10.1007/978-3-319-26432-5)
- Gosling, J. T. 2012, *SSRv*, 172, 187, doi: [10.1007/s11214-011-9747-2](https://doi.org/10.1007/s11214-011-9747-2)
- Greco, A., Chuychai, P., Matthaeus, W. H., Servidio, S., & Dmitruk, P. 2008, *Geophys. Res. Lett.*, 35, L19111, doi: [10.1029/2008GL035454](https://doi.org/10.1029/2008GL035454)
- Greco, A., Matthaeus, W. H., Servidio, S., Chuychai, P., & Dmitruk, P. 2009, *ApJL*, 691, L111, doi: [10.1088/0004-637X/691/2/L111](https://doi.org/10.1088/0004-637X/691/2/L111)
- Greco, A., Perri, S., Servidio, S., Yordanova, E., & Veltri, P. 2016, *ApJL*, 823, L39, doi: [10.3847/2041-8205/823/2/L39](https://doi.org/10.3847/2041-8205/823/2/L39)
- Guo, Z., Lin, Y., & Wang, X. 2021a, *Journal of Geophysical Research (Space Physics)*, 126, e28853, doi: [10.1029/2020JA028853](https://doi.org/10.1029/2020JA028853)
- Guo, Z., Lin, Y., Wang, X., & Du, A. 2018, *Journal of Geophysical Research (Space Physics)*, 123, 9169, doi: [10.1029/2018JA025679](https://doi.org/10.1029/2018JA025679)

- . 2021b, *Journal of Geophysical Research (Space Physics)*, 126, e29979, doi: [10.1029/2021JA029979](https://doi.org/10.1029/2021JA029979)
- Guo, Z., Lin, Y., Wang, X., et al. 2020, *Journal of Geophysical Research (Space Physics)*, 125, e27795, doi: [10.1029/2020JA027795](https://doi.org/10.1029/2020JA027795)
- Haaland, S., & Gjerloev, J. 2013, *Journal of Geophysical Research: Space Physics*, 118, 7593
- Haaland, S., Reistad, J., Tenfjord, P., et al. 2014, *J. Geophys. Res.*, 119, 9019, doi: [10.1002/2014JA020539](https://doi.org/10.1002/2014JA020539)
- Hada, T., Kennel, C. F., & Buti, B. 1989, *J. Geophys. Res.*, 94, 65, doi: [10.1029/JA094iA01p00065](https://doi.org/10.1029/JA094iA01p00065)
- Harteringer, M. D., Turner, D. L., Plaschke, F., Angelopoulos, V., & Singer, H. 2013, *J. Geophys. Res.*, 118, 299, doi: [10.1029/2012JA018349](https://doi.org/10.1029/2012JA018349)
- Hasegawa, H. 2012, *Monographs on Environment, Earth and Planets*, 1, 71, doi: [10.5047/meep.2012.00102.0071](https://doi.org/10.5047/meep.2012.00102.0071)
- Hietala, H., Phan, T. D., Angelopoulos, V., et al. 2018, *Geophys. Res. Lett.*, 45, 1732, doi: [10.1002/2017GL076525](https://doi.org/10.1002/2017GL076525)
- Hubert, D., & Harvey, C. C. 2000, *Geophys. Res. Lett.*, 27, 3149, doi: [10.1029/2000GL003776](https://doi.org/10.1029/2000GL003776)
- Hudson, P. D. 1970, *Planet. Space Sci.*, 18, 1611, doi: [10.1016/0032-0633\(70\)90036-X](https://doi.org/10.1016/0032-0633(70)90036-X)
- Jacobsen, K. S., Phan, T. D., Eastwood, J. P., et al. 2009, *Journal of Geophysical Research (Space Physics)*, 114, A08210, doi: [10.1029/2008JA013873](https://doi.org/10.1029/2008JA013873)
- Kennel, C. F., Mal'Kov, M. A., Sagdeev, R. Z., Shapiro, V. D., & Khrabrov, A. V. 1988, *Soviet Journal of Experimental and Theoretical Physics Letters*, 48, 79
- Knetter, T., Neubauer, F. M., Horbury, T., & Balogh, A. 2004, *J. Geophys. Res.*, 109, A06102, doi: [10.1029/2003JA010099](https://doi.org/10.1029/2003JA010099)
- Kropotina, J. A., Webster, L., Artemyev, A. V., et al. 2021, *ApJ*, 913, 142, doi: [10.3847/1538-4357/abf6c7](https://doi.org/10.3847/1538-4357/abf6c7)
- Landau, L. D., & Lifshitz, E. M. 1960, Vol. 8: *Electrodynamics of Continuous Media, Course of Theoretical Physics (Pergamon Press)*
- Lin, Y. 1997, *J. Geophys. Res.*, 102, 24265, doi: [10.1029/97JA01989](https://doi.org/10.1029/97JA01989)
- . 2002, *Planet. Space Sci.*, 50, 577, doi: [10.1016/S0032-0633\(02\)00037-5](https://doi.org/10.1016/S0032-0633(02)00037-5)
- Lin, Y. 2003, *Journal of Geophysical Research: Space Physics*, 108
- Lin, Y., & Lee, L. C. 1993, *SSRv*, 65, 59, doi: [10.1007/BF00749762](https://doi.org/10.1007/BF00749762)
- Lin, Y., Lee, L. C., & Yan, M. 1996a, *J. Geophys. Res.*, 101, 479, doi: [10.1029/95JA02985](https://doi.org/10.1029/95JA02985)
- Lin, Y., Swift, D. W., & Lee, L. C. 1996b, *J. Geophys. Res.*, 101, 27251, doi: [10.1029/96JA02733](https://doi.org/10.1029/96JA02733)
- Lin, Y., & Wang, X. Y. 2005, *Journal of Geophysical Research (Space Physics)*, 110, A12216, doi: [10.1029/2005JA011243](https://doi.org/10.1029/2005JA011243)
- Liu, Z., Turner, D. L., Angelopoulos, V., & Omidi, N. 2015, *Geophys. Res. Lett.*, 42, 7860, doi: [10.1002/2015GL065842](https://doi.org/10.1002/2015GL065842)
- Loureiro, N. F., & Boldyrev, S. 2017, *PhRvL*, 118, 245101, doi: [10.1103/PhysRevLett.118.245101](https://doi.org/10.1103/PhysRevLett.118.245101)
- Loureiro, N. F., Schekochihin, A. A., & Cowley, S. C. 2007, *Physics of Plasmas*, 14, 100703, doi: [10.1063/1.2783986](https://doi.org/10.1063/1.2783986)
- Lukin, A. S., Artemyev, A. V., Petrukovich, A. A., et al. 2019, *Journal of Geophysical Research (Space Physics)*, 124, 5027, doi: [10.1029/2019JA026638](https://doi.org/10.1029/2019JA026638)
- Lyubarsky, Y., & Kirk, J. G. 2001, *ApJ*, 547, 437, doi: [10.1086/318354](https://doi.org/10.1086/318354)
- Malkov, M. A., Kennel, C. F., Wu, C. C., Pellat, R., & Shapiro, V. D. 1991, *Physics of Fluids B*, 3, 1407, doi: [10.1063/1.859706](https://doi.org/10.1063/1.859706)
- Matsumoto, Y., Amano, T., Kato, T. N., & Hoshino, M. 2015, *Science*, 347, 974, doi: [10.1126/science.1260168](https://doi.org/10.1126/science.1260168)
- Matthaeus, W. H., Wan, M., Servidio, S., et al. 2015, *Philosophical Transactions of the Royal Society of London A: Mathematical, Physical and Engineering Sciences*, 373, doi: [10.1098/rsta.2014.0154](https://doi.org/10.1098/rsta.2014.0154)
- McFadden, J. P., Carlson, C. W., Larson, D., et al. 2008, *SSRv*, 141, 277, doi: [10.1007/s11214-008-9440-2](https://doi.org/10.1007/s11214-008-9440-2)
- Medvedev, M. V., Shevchenko, V. I., Diamond, P. H., & Galinsky, V. L. 1997, *Physics of Plasmas*, 4, 1257, doi: [10.1063/1.872356](https://doi.org/10.1063/1.872356)
- Neugebauer, M. 2006, *J. Geophys. Res.*, 111, A04103, doi: [10.1029/2005JA011497](https://doi.org/10.1029/2005JA011497)
- Newman, R., Vainchtein, D., & Artemyev, A. 2020, *Solar Physics*, 295, 129, doi: [10.1007/s11207-020-01695-z](https://doi.org/10.1007/s11207-020-01695-z)

- Ng, J., Chen, L. J., & Omelchenko, Y. A. 2021, *Physics of Plasmas*, 28, 092902, doi: [10.1063/5.0054394](https://doi.org/10.1063/5.0054394)
- Omidi, N., Berchem, J., Sibeck, D., & Zhang, H. 2016, *Journal of Geophysical Research (Space Physics)*, 121, 3155, doi: [10.1002/2015JA022170](https://doi.org/10.1002/2015JA022170)
- Omidi, N., Lee, S. H., Sibeck, D. G., et al. 2020, *Journal of Geophysical Research (Space Physics)*, 125, e28058, doi: [10.1029/2020JA028058](https://doi.org/10.1029/2020JA028058)
- Omidi, N., Sibeck, D., Blanco-Cano, X., et al. 2013, *Journal of Geophysical Research (Space Physics)*, 118, 823, doi: [10.1002/jgra.50146](https://doi.org/10.1002/jgra.50146)
- Omidi, N., & Sibeck, D. G. 2007, *Journal of Geophysical Research (Space Physics)*, 112, A01203, doi: [10.1029/2006JA011663](https://doi.org/10.1029/2006JA011663)
- Omidi, N., Sibeck, D. G., & Blanco-Cano, X. 2009, *Journal of Geophysical Research (Space Physics)*, 114, A08205, doi: [10.1029/2008JA013950](https://doi.org/10.1029/2008JA013950)
- Pang, Y., Lin, Y., Deng, X. H., Wang, X. Y., & Tan, B. 2010, *Journal of Geophysical Research (Space Physics)*, 115, A03203, doi: [10.1029/2009JA014415](https://doi.org/10.1029/2009JA014415)
- Parker, E. N. 1957, *J. Geophys. Res.*, 62, 509, doi: [10.1029/JZ062i004p00509](https://doi.org/10.1029/JZ062i004p00509)
- Paschmann, G., Baumjohann, W., Sckopke, N., Papamastorakis, I., & Carlson, C. W. 1986, *J. Geophys. Res.*, 91, 11099, doi: [10.1029/JA091iA10p11099](https://doi.org/10.1029/JA091iA10p11099)
- Paschmann, G., Øieroset, M., & Phan, T. 2013, *SSRv*, 178, 385, doi: [10.1007/s11214-012-9957-2](https://doi.org/10.1007/s11214-012-9957-2)
- Paschmann, G., Papamastorakis, I., Sckopke, N., et al. 1979, *Nature*, 282, 243, doi: [10.1038/282243a0](https://doi.org/10.1038/282243a0)
- Pecora, F., Servidio, S., Greco, A., et al. 2018, *Journal of Plasma Physics*, 84, 725840601, doi: [10.1017/S0022377818000995](https://doi.org/10.1017/S0022377818000995)
- Petschek, H. E. 1964, *NASA Special Publication*, 50, 425
- Phan, T., Paschmann, G., Gosling, J., et al. 2013, *Geophysical Research Letters*, 40, 11
- Phan, T. D., Gosling, J. T., Davis, M. S., et al. 2006, *Nature*, 439, 175, doi: [10.1038/nature04393](https://doi.org/10.1038/nature04393)
- Phan, T. D., Paschmann, G., Twitty, C., et al. 2007, *Geophys. Res. Lett.*, 34, L14104, doi: [10.1029/2007GL030343](https://doi.org/10.1029/2007GL030343)
- Phan, T. D., Drake, J. F., Shay, M. A., et al. 2014, *Geophys. Res. Lett.*, 41, 7002, doi: [10.1002/2014GL061547](https://doi.org/10.1002/2014GL061547)
- Podesta, J. J. 2017, *J. Geophys. Res.*, 122, 2795, doi: [10.1002/2016JA023629](https://doi.org/10.1002/2016JA023629)
- Pollock, C., Moore, T., Jacques, A., et al. 2016, *SSRv*, 199, 331, doi: [10.1007/s11214-016-0245-4](https://doi.org/10.1007/s11214-016-0245-4)
- Pontin, D. I., & Priest, E. R. 2022, *Living Reviews in Solar Physics*, 19, 1, doi: [10.1007/s41116-022-00032-9](https://doi.org/10.1007/s41116-022-00032-9)
- Pucci, F., & Velli, M. 2014, *ApJL*, 780, L19, doi: [10.1088/2041-8205/780/2/L19](https://doi.org/10.1088/2041-8205/780/2/L19)
- Roth, M., de Keyser, J., & Kuznetsova, M. M. 1996, *Space Science Reviews*, 76, 251, doi: [10.1007/BF00197842](https://doi.org/10.1007/BF00197842)
- Russell, C. T., Anderson, B. J., Baumjohann, W., et al. 2016, *SSRv*, 199, 189, doi: [10.1007/s11214-014-0057-3](https://doi.org/10.1007/s11214-014-0057-3)
- Samsonov, A. A., Alexandrova, O., Lacombe, C., Maksimovic, M., & Gary, S. P. 2007, *Annales Geophysicae*, 25, 1157, doi: [10.5194/angeo-25-1157-2007](https://doi.org/10.5194/angeo-25-1157-2007)
- Servidio, S., Greco, A., Matthaeus, W. H., Osman, K. T., & Dmitruk, P. 2011a, *J. Geophys. Res.*, 116, 9102, doi: [10.1029/2011JA016569](https://doi.org/10.1029/2011JA016569)
- Servidio, S., Dmitruk, P., Greco, A., et al. 2011b, *Nonlinear Processes in Geophysics*, 18, 675, doi: [10.5194/npg-18-675-2011](https://doi.org/10.5194/npg-18-675-2011)
- Shi, F., Lin, Y., Wang, X., Wang, B., & Nishimura, Y. 2021, *Earth, Planets and Space*, 73, 138, doi: [10.1186/s40623-021-01469-2](https://doi.org/10.1186/s40623-021-01469-2)
- Shue, J.-H., Chao, J. K., Fu, H. C., et al. 1997, *J. Geophys. Res.*, 102, 9497, doi: [10.1029/97JA00196](https://doi.org/10.1029/97JA00196)
- Sibeck, D. G., Lee, S. H., Omidi, N., & Angelopoulos, V. 2021, *Journal of Geophysical Research (Space Physics)*, 126, e29201, doi: [10.1029/2021JA029201](https://doi.org/10.1029/2021JA029201)
- Sibeck, D. G., Phan, T. D., Lin, R., Lepping, R. P., & Szabo, A. 2002, *Journal of Geophysical Research (Space Physics)*, 107, 1271, doi: [10.1029/2001JA007539](https://doi.org/10.1029/2001JA007539)
- Sibeck, D. G., Kudela, K., Lepping, R. P., et al. 2000, *J. Geophys. Res.*, 105, 25155, doi: [10.1029/2000JA900109](https://doi.org/10.1029/2000JA900109)
- Sironi, L., & Spitkovsky, A. 2011, *ApJ*, 741, 39, doi: [10.1088/0004-637X/741/1/39](https://doi.org/10.1088/0004-637X/741/1/39)
- . 2012, *Computational Science and Discovery*, 5, 014014, doi: [10.1088/1749-4699/5/1/014014](https://doi.org/10.1088/1749-4699/5/1/014014)



- Söding, A., Neubauer, F. M., Tsurutani, B. T., Ness, N. F., & Lepping, R. P. 2001, *Annales Geophysicae*, 19, 681
- Sonnerup, B. U. Ö., & Scheible, M. 2000, ESA Special Publication, Vol. 449, ISSI Book on Analysis Methods for Multi-Spacecraft Data, ed. G.Paschmann and Patrick W. D.
- Spitkovsky, A. 2006, *ApJL*, 648, L51, doi: [10.1086/507518](https://doi.org/10.1086/507518)
- Swisdak, M., & Drake, J. 2007, *Geophysical Research Letters*, 34
- Syrovatskii, S. I. 1981, *Annual review of astronomy and astrophysics*, 19, 163, doi: [10.1146/annurev.aa.19.090181.001115](https://doi.org/10.1146/annurev.aa.19.090181.001115)
- Tan, B., Lin, Y., Perez, J. D., & Wang, X. Y. 2011, *Journal of Geophysical Research (Space Physics)*, 116, A02206, doi: [10.1029/2010JA015580](https://doi.org/10.1029/2010JA015580)
- Tsurutani, B. T., & Ho, C. M. 1999, *Reviews of Geophysics*, 37, 517, doi: [10.1029/1999RG900010](https://doi.org/10.1029/1999RG900010)
- Uzdensky, D. A., Cerutti, B., & Begelman, M. C. 2011, *ApJL*, 737, L40, doi: [10.1088/2041-8205/737/2/L40](https://doi.org/10.1088/2041-8205/737/2/L40)
- Vasko, I. Y., Alimov, K., Phan, T. D., et al. 2021, *ApJL*, 923, L19, doi: [10.3847/2041-8213/ac3f30](https://doi.org/10.3847/2041-8213/ac3f30)
- Vasquez, B. J., Abramenko, V. I., Haggerty, D. K., & Smith, C. W. 2007, *Journal of Geophysical Research (Space Physics)*, 112, A11102, doi: [10.1029/2007JA012504](https://doi.org/10.1029/2007JA012504)
- Vasquez, B. J., & Hollweg, J. V. 1999, *J. Geophys. Res.*, 104, 4681, doi: [10.1029/1998JA900090](https://doi.org/10.1029/1998JA900090)
- . 2001, *J. Geophys. Res.*, 106, 5661, doi: [10.1029/2000JA000268](https://doi.org/10.1029/2000JA000268)
- Vörös, Z., Varsani, A., Yordanova, E., et al. 2021, *Journal of Geophysical Research (Space Physics)*, 126, e29415, doi: [10.1029/2021JA029415](https://doi.org/10.1029/2021JA029415)
- Vörös, Z., Yordanova, E., Varsani, A., et al. 2017, *Journal of Geophysical Research (Space Physics)*, 122, 11,442, doi: [10.1002/2017JA024535](https://doi.org/10.1002/2017JA024535)
- Vu, A., Liu, T. Z., Zhang, H., & Pollock, C. 2022, *Journal of Geophysical Research (Space Physics)*, 127, e30029, doi: [10.1029/2021JA030029](https://doi.org/10.1029/2021JA030029)
- Wang, B., Nishimura, Y., Hietala, H., et al. 2018a, *Journal of Geophysical Research (Space Physics)*, 123, 6347, doi: [10.1029/2017JA024846](https://doi.org/10.1029/2017JA024846)
- Wang, B., Liu, T., Nishimura, Y., et al. 2020a, *Journal of Geophysical Research (Space Physics)*, 125, e28411, doi: [10.1029/2020JA028411](https://doi.org/10.1029/2020JA028411)
- Wang, C.-P., Liu, T. Z., Xing, X., & Masson, A. 2018b, *Journal of Geophysical Research (Space Physics)*, 123, 9381, doi: [10.1029/2018JA025921](https://doi.org/10.1029/2018JA025921)
- . 2018c, *Journal of Geophysical Research (Space Physics)*, 123, 9381, doi: [10.1029/2018JA025921](https://doi.org/10.1029/2018JA025921)
- Wang, C.-P., Wang, X., Liu, T. Z., & Lin, Y. 2020b, *Geophys. Res. Lett.*, 47, e89844, doi: [10.1029/2020GL089844](https://doi.org/10.1029/2020GL089844)
- . 2020c, *Geophys. Res. Lett.*, 47, e89844, doi: [10.1029/2020GL089844](https://doi.org/10.1029/2020GL089844)
- Wang, C.-P., Zaharia, S. G., Lyons, L. R., & Angelopoulos, V. 2013, *J. Geophys. Res.*, 118, 244, doi: [10.1029/2012JA018275](https://doi.org/10.1029/2012JA018275)
- Wang, S., Chen, L.-J., Bessho, N., et al. 2019, *Geophys. Res. Lett.*, 46, 562, doi: [10.1029/2018GL080944](https://doi.org/10.1029/2018GL080944)
- Webster, L., Vainchtein, D., & Artemyev, A. 2021, *SoPh*, 296, 87, doi: [10.1007/s11207-021-01824-2](https://doi.org/10.1007/s11207-021-01824-2)
- Wright, A. N., & Elsdén, T. 2020, *Journal of Geophysical Research: Space Physics*, 125, e2019JA027589, doi: [10.1029/2019JA027589](https://doi.org/10.1029/2019JA027589)
- Wu, D. J., Chao, J. K., & Lepping, R. P. 2000, *J. Geophys. Res.*, 105, 12627, doi: [10.1029/1999JA000265](https://doi.org/10.1029/1999JA000265)
- Yan, M., & Lee, L. C. 1996, *J. Geophys. Res.*, 101, 4835, doi: [10.1029/95JA02976](https://doi.org/10.1029/95JA02976)
- Zhang, X. J., Angelopoulos, V., Artemyev, A. V., Hartinger, M. D., & Bortnik, J. 2020, *Journal of Geophysical Research (Space Physics)*, 125, e28334, doi: [10.1029/2020JA028334](https://doi.org/10.1029/2020JA028334)